8-22-2011

Experimental and Numerical Investigations of Tubular-Shaped Direct Methanol Fuel Cells (DMFCs)

Travis R. Ward
University of Connecticut - Storrs, traviswards@gmail.com

Experimental and Numerical Investigations of Tubular-Shaped Direct Methanol Fuel Cells (DMFCs)

Travis Robert Ward

B.S., University of Connecticut, 2008

A Thesis

Submitted in Partial Fulfillment of the

Requirement for the Degree of

Masters of Science

at the

University of Connecticut

2011

Certificate of Approval

Master of Science Thesis

Experimental and Numerical Investigations of Tubular-Shaped Direct Methanol Fuel Cells (DMFCs)

Presented by:

Travis Robert Ward

Major Advisor_____

Amir Faghri

Associate Advisor_____

Theodore Bergman

Associate Advisor_____

Tai-Hsi Fan

Associate Advisor_____

Ugur Pasaogullari

University of Connecticut

2011

Acknowledgements

I would personally like to take this opportunity to thank those who have contributed to my Master's thesis work along the way; without you, none of this would have been possible.

Dr. Amir Faghri, my Advisor throughout the past two years: thank you for providing me with the opportunity to be involved in an exciting field conducting investigative research on tubular-shaped fuel cells. With your rigorous expectations, support and guidance I have gained new skills and knowledge that will no doubt help me in my future career as an engineer.

Dr.Theodore Bergman, Dr. Tai-Hsi Fan, and Dr. Ugur Pasaogullari, my Associate Advisors: I am grateful for your individual suggestions and valuable advice.

To all my Lab-mates: I cannot thank you enough for providing me constant instruction, an open ear, assisting with the editing of my papers, and your enthusiasm, friendship and encouragement throughout my Master's career.

To Mark Drobney, a Mechanical Specialist at the Biotehcnology/Bioservices Center located on the Depot Campus. Mark provided valuable advice and experience in machining the different tubular fuel cell frame iterations used in the experimental work presented in this thesis.

Lastly, to my family, friends, and girlfriend Katie for your support, full-hearted understanding, and love.

Table of Contents

List of Figures

List of Tables

Abstract

This study focuses on both the numerical and experimental investigations of the novel, passively operated, tubular-shaped, Direct Methanol Fuel Cell (DMFC) as an alternative geometry to the traditional planar-shaped fuel cell. The DMFC has grown in popularity due to its high energy density (liquid methanol fuel), low emissions, passive operation, safe handling, and small-scale portable power generation capabilities. The benefit of the tubular geometry compared to the planar geometry is the higher instantaneous volumetric power density provided by the larger active area, which could be beneficial in applications that require a high instantaneous power while occupying a small volume.

A two-dimensional, two-phase, non-isothermal model was developed to investigate the steady-state performance and design characteristics of a tubular-shaped, passive DMFC. It was found that by increasing the ambient temperature surrounding the fuel cell from 20 to 40 ºC increases the peak power density produced by the fuel cell by 11.3 mW cm^{-2} with 1 M, 16.3 mW cm^{-2} with 2 M, but by only 8.4 mW cm^{-2} with 3 M methanol. The poor performance with 3 M methanol at a higher ambient temperature is caused by increased methanol crossover and significant oxygen depletion along the Cathode Transport Layer (CTL). For a 5 cm long tubular DMFC to maintain sufficient Oxygen transport, the thickness of the CTL must be greater than 1 mm for 1 M operation, greater than 5 mm for 2 M operation, and greater than 10 mm for 3 M or higher operation.

Secondly, a tubular-shaped DMFC frame was built that operated completely passively with methanol solution stored in a central fuel reservoir and external axial

channels that allowed passive air flow. Membrane Electrode Assemblies (MEAs), with identical compositions, were installed in both tubular and planar-shaped, passive DMFCs and tested with 1, 2, and 3 M methanol solutions at room temperature in order to compare the performance of the tubular geometry to the planar geometry. The peak power density for the tubular DMFC was 19.0 mW cm^{-2} and 24.5 mW cm^{-2} while the peak power density for the planar DMFC was 20.0 mW cm^{-2} and 23.0 mW cm^{-2} with Nafion® 212 and 115 MEAs, respectively. Even though the performance of the fuel cell improved with each increase in Methanol concentration, the fuel and energy efficiencies decreased for both the tubular and planar geometries due to increased Methanol crossover. The tubular DMFC experienced higher methanol crossover potentially due to a higher static fluid pressure in the Anode Fuel Reservoir (AFR) caused by the vertical orientation of the tubular fuel reservoir. The performance of the tubular DMFC in this work represents an 870 % improvement in power density from the previous best, passive, tubular DMFC found in the literature.

Keywords: Direct Methanol Fuel Cell, Tubular, Passive, Fuel Efficiency, Energy Efficiency, Performance

Chapter 1. Introduction

1.1. History of fuel cells

Fuel Cells are considered to be one of the major energy conversion technologies for the future, due to the unique advantages of electrochemical energy conversion processes compared to the existing thermal combustion energy conversion processes available today. Over the last century fuel cells have gained significant interest among the energy sector due to their high efficiency energy conversion and environmental benefits.

The idea of a "gaseous voltaic battery" or later known as a fuel cell originally surfaced in 1839 from William Robert Grove [1]. He proved that a fuel cell operating on Hydrogen and Oxygen and consisting of electrodes with a Platinum coating immersed in Sulfuric Acid would produce electricity. In general, a fuel cell is an electrochemical device that continuously converts the free energy available from a chemical reaction of a fuel (and oxidant) directly into electrical energy. Additional by-products of the chemical reaction in a fuel cell consist of heat, water, carbon dioxide, and lower forms of hydrocarbons depending on the type of fuel used in the reaction and the type of fuel cell operating. Figure 1.1 shows a generic system described by a fuel cell including the inputs and outputs.

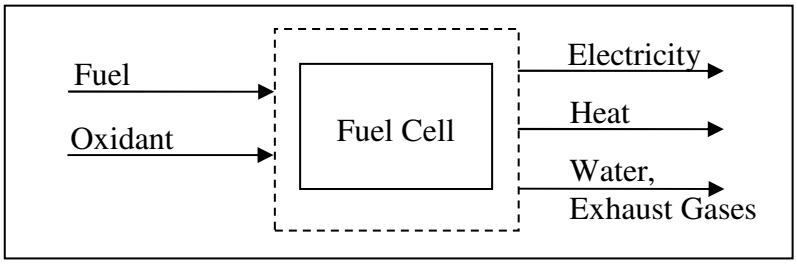

Figure 1.1: Fuel Cell System

Unlike a thermal engine, since there is no combustion in a fuel cell there are no NO_x emissions. Also, since sulfur acts as a poison to all types of fuel cells it must be removed from the fuel before it can be fed to the fuel cell, thus there is no SO_x generated as well [1].

A fuel cell is very similar to a battery since they both output electricity from an electrochemical reaction between fuel and an oxidant. In this since, scientists talk about fuel cells and batteries being interchangeable sources of energy. The difference between a fuel cell and a battery is that a fuel cell is an open system and a battery is a closed system. A battery is used to store then give off energy while a fuel cell produces energy. Batteries have a limited amount of energy they can output based on the amount of chemical reactants stored in the battery. As the opposite ends of a battery are connected, the battery begins to discharge and electrons flow along the external circuit. The battery will eventually run out of reactants and stop producing power. At this point the battery must either be thrown away or recharged from an external electrical power supply. In other words, a battery is simply a container that stores energy until it is needed at a later time. A fuel cell takes in fuel and oxidants then converts the chemical energy in the fuel into useful electrical energy. As long as reactants are supplied to a fuel cell it will continue to produce energy. Unlike batteries, fuel cells do not run out of energy and don't need to be thrown away after each use. This is promising, because fuel cells have the potential to replace batteries with constant on-board power generation units.

Similarly to fuel cells, heat engines convert chemical energy, available in fuel, into electrical energy. The main difference between the conversion from chemical to electrical energy in a heat engine compared to a fuel cell is that a heat engine requires

several intermediate steps to complete the energy transformation. Both heat engines and fuel cells operate best at certain temperatures that are favorable to the chemical reactions that occur in their respective systems. In a heat engine, first chemical energy is converted to thermal energy as the fuel is combusted. Next, a heat engine converts the thermal energy into mechanical energy and finally the mechanical energy is converted into electrical energy with an electric generator (turbine). The efficiency of a heat engine is limited by Carnot's Law, which says the maximum efficiency of a heat engine is related to the temperature ratio between the hot and cold reservoirs. Since there are several moving parts in the process of converting chemical to electrical energy with a heat engine, there is significant wear over time as well as opportunities for the overall efficiency of the system to decrease. All of the components must be regularly serviced to maintain optimum efficiency. Fuel cells operate without moving parts so they have very little maintenance cost and the efficiency of fuel cells is much higher than heat engines since they are not limited by Carnot's Law.

Since fuel cells are not limited by Carnot's Law, the maximum theoretical efficiency of a fuel cell is significantly higher than that of a heat engine. Theoretically, a fuel cell can achieve 55-65% energy efficiency when operating as Combined Heat and Power (CHP) producing both power (electricity) and heating water to heat a facility or run a turbine to produce further power [1]. Fuel cells also allow convenient on-site power generation that would reduce costly transmission lines and associated transmission losses during power distribution from existing power plants. Fuel cell systems contain few or no moving parts, which significantly increase their reliability compared to combustion

engines and power plants. Figure 1.2 provides a general schematic of electricity production from both thermal (heat) engines and fuel cells as comparison.

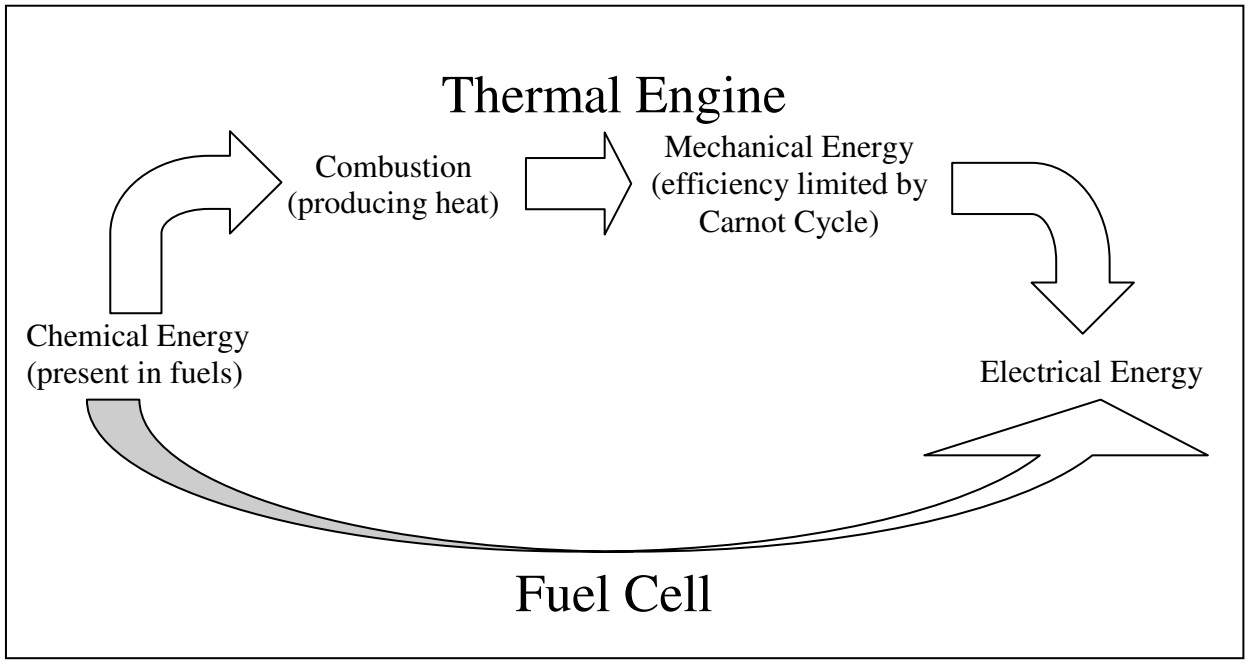

Figure 1.2: Electricity Production from a Thermal Engine vs. a Fuel Cell

The basic components of a fuel cell are the anode, cathode, electrolyte, bipolar plates/ current collectors, and a frame or gaskets used for sealing and holding all of the components together. At the anode, fuel is oxidized while at the cathode, oxidant is reduced. Examples of fuels include: H_2, N_2H_4, NH_3, CH_3OH, coal gas, or even hydrocarbons, while pure Oxygen or air are used as oxidants. The anode and cathode are both electrodes made from porous electrically conductive material with a layer of catalyst. Platinum (Pt) is the most popular catalyst for low temperature fuel cells while nickel is the most popular catalyst for high temperature fuel cells. Other materials are also used depending on the type of fuel. An electrolyte separates the anode and cathode sides of the fuel cell and is made from a material that promotes high ionic conductivity and no (or very little) electron conductivity.

There are several different types of fuel cells that are classified by the nature of their electrolyte and also by their operating temperature. Thus, one can separate fuel cells as either alkaline (basic) or acidic or as low temperature (up to 100 ºC), medium temperature (up to 200 ºC), and high temperature (up to 1000 ºC) fuel cells. Table 1.1 provides a breakdown of the major types of fuel cells along with their respective fuels, electrolyte materials, and oxidants. The specific fuel cells shown below include the: Polymer Electrolyte Membrane Fuel Cell (PEMFC), Direct Methanol Fuel Cell (DMFC), Phosphoric Acid Fuel Cell (PAFC), Alkaline Fuel Cell (AFC), Solid Oxide Fuel Cell (SOFC), and Molten Carbonate Fuel Cell (MCFC). These fuel cells are the most popular among the research community and also commercially produced. As seen in Table 1.1, all fuel cells operate with Oxygen as their oxidant and most can operate with air providing the necessary Oxygen to complete the reaction at the cathode. The AFC

requires oxygen gas at the cathode, because Carbon Dioxide poisons the electrolyte by reacting with the liquid Potassium Hydroxide (KOH) electrolyte and converting it to Carbonate among other products. This reaction makes the cell impractical for use as a power source. As a result, either Carbon Dioxide must be "scrubbed" from the incoming air before it contacts the cathode side of the fuel cell, or Oxygen must directly be used as an oxidant in this type of fuel cell [2]. The MCFC must operate with a combination of both air and Carbon Dioxide as the oxidant, because Carbon Dioxide is used in the reaction at the cathode to produce Carbonate CO_3^{2-} ions that transport across the electrolyte to be used in the anode reaction. One mole of Carbon Dioxide is transformed to a Carbonate ion in the cathode. One Carbonate ion is transferred from the cathode, through the ceramic electrolyte layer, to the anode for every 2 moles of electrons that are transferred out of the cell as electricity [1].

Table 1.1: Fuels, Oxidants, and Electrolyte Materials for Common Fuel Cells

	Anode	Electrolyte	Cathode
	Fuel	**Material**	**Oxidant**
PEMFC	H_2 gas	Polymer Plastic Membrane	Air
DMFC	Methanol	Polymer Plastic Membrane	Air
PAFC	H_2 gas	100% Phosphoric Acid	Air
AFC	H_2 gas	Concentrated KOH (30-50%) in H_2O	Oxygen Gas
SOFC	Hydrocarbons	Yttrium- Stabilized Zirkondioxide	Air
MCFC	Hydrocarbons	Molten Carbonate in $LiAlO_2$ ceramic matrix	Air + CO_2

In general, the nature of the oxidant as well as the type of fuel, set restrictions on the operating conditions of the various fuel cell types. PEMFCs, PAFCs, and DMFCs are considered to be acidic fuel cells that can utilize air, as well as Oxygen, as an oxidant. AFCs must operate with pure Oxygen so as to avoid Carbonization of the alkaline electrolyte. Most of the PEMFCs, as well as DMFCs and AFCs operate at temperatures up to 100 ºC, while some new, improved PEMFCs, with the addition of a modified high-temperature polymer membrane, can operate above 100 ºC. PAFCs, with working temperatures around 200 ºC, can tolerate fuels with CO levels in the range of several hundred ppm, in contrast to PEMFCs with platinum-based anodes, which require high purity Hydrogen or "scrubbed" fuel [1]. When hydrocarbon fuel is reformed to produce Hydrogen for PEMFCs, one of the by-products is Carbon Monoxide (CO) in the Hydrogen gas stream. Thus, operating PEMFCs with Hydrogen gas that contains CO, as well as DMFCs fed with liquid Methanol which produce CO during catalysis, require anode catalysts with high tolerance to CO. Several new catalysts have been derived that can tolerate CO, but the most popular CO tolerant catalyst remains Platinum-Ruthenium (Pt-Ru) widely used in the DMFC. With the addition of Pt-Ru catalyst rather than just Pt to the anode, during the reaction of liquid Methanol, Ru blocks CO attachment sites on the Pt particles, thus allowing fuel to continue to attach and react at the Pt catalyst sites instead of CO. MCFCs and SOFCs are considered to be high-temperature fuel cells, and can operate with a variety of fuels other than Hydrogen, for example Methane and natural gas, since the high temperature operation is able to automatically reform fuel into Hydrogen gas during operation. Also, the high temperature operation of these fuel cells makes them very tolerable to CO and other poisons.

1.2. Direct methanol fuel cell

This paper focuses on one specific type of fuel cell, the DMFC, which is a type of PEMFC. As a direct result of recent developments in portable, hand-held technology that demands larger outputs in power density and new, alternate sources of energy, the DMFC has gained a lot of attention due to its higher energy density compared to Lithium Ion batteries. The DMFC operates at low temperatures, gives off low emissions, is based on a simple geometry that can provide completely passive energy, and methanol, its fuel, provides high energy content along with safe storage capabilities [3]. There are two basic half-reactions that occur in a DMFC:

-Liquid methanol and water are broken into protons, electrons, and carbon dioxide gas at the Anode Catalyst Layer (ACL):

$$CH_3OH + H_2O \rightarrow 6H^+ + 6e^- + CO_2 \quad (1)$$

-Oxygen gas, protons, and electrons are converted into water at the Cathode Catalyst Layer (CCL):

$$\frac{3}{2}O_2 + 6H^+ + 6e^- \rightarrow 3H_2O \quad (2)$$

-The overall reaction is:

$$CH_3OH + \frac{3}{2}O_2 \rightarrow 2H_2O + CO_2 \quad (3)$$

There are three main types of DMFCs: active, semi-passive, and passive. An active DMFC requires external pumps and fans to force the flow of methanol and oxygen to the fuel cell. This type of DMFC produces the highest power density (as a result of always having sufficient fuel or oxidant in the catalyst layers), but the addition of auxiliary components (pumps, fans, heaters, external humidity equipment) reduces the

overall theoretical efficiency of the fuel cell since they require electricity to run. A semi-passive DMFC operates with an active anode and passive cathode or a passive anode and active cathode. On the other hand, a passive DMFC operates completely on its own. Methanol is mainly transported to the ACL due to concentration gradients and gravity which force the fuel through porous diffusion layers (Anode Diffusion Layer (ADL) and Anode Micro-Porous Layer (AMPL)) that provide mass transport resistance, while oxygen is readily provided from the air and transported by natural convection and diffusion to the CCL.

There have been extensive experimental research efforts discussing the development and subsequent improvement of passive, planar DMFCs. One large problem hindering the commercialization of DMFCs is methanol crossover, which can be resolved by utilizing dilute methanol at the anode instead of high concentration or "neat" methanol. Dilute methanol has substantially less energy density compared to neat methanol since there is less fuel available to be used by the fuel cell. As a result, a larger Anode Fuel Reservoir (AFR) is necessary to provide sufficient water to dilute the methanol fuel and prevent crossover, while also providing sufficient fuel to power the fuel cell. The DMFC has been considered a potential replacement for small, portable power applications, which means the final product (the fuel cell and AFR) must remain compact and capable of fitting in the current space occupied by Lithium Ion batteries. It is worthwhile to note that in passive DMFCs that are designed for portable applications, there is no additional fuel reservoir that accompanies the fuel cell. The fuel reservoir is built into the fuel cell assembly.

1.2.1. Tubular-shaped DMFC

Previously, most DMFC research efforts were focused on planar, flat geometries. This work considers a tubular DMFC geometry that has the anode on the inside of the tube and the cathode on the outside of the tube. Considering a fuel cell that produces the same voltage and current density, independent of the geometry, which is a valid assumption if the same Membrane Electrode Assembly (MEA) and fuel are used to build and operate both a tubular and a planar DMFC; a tubular shaped fuel cell has several distinct advantages over a planar-shaped fuel cell:

- For certain geometric conditions, the tubular DMFC has a higher instantaneous Volumetric Power Density (VPD) than the planar DMFC associated with higher instantaneous power output per unit volume.
- Ability to operate in all orientations without lack of methanol contacting the ACL.
- Reduced cost due to decreased volume of materials.
- Same shape as existing AA, AAA, D, and C batteries, which allows easier conversion between batteries and fuel cells in the future.
- With the elimination of flow fields at the cathode, uniform pressure is applied across the membrane electrode assembly (MEA) [4].

Based on these significant advantages, the passive, tubular DMFC should be considered a potential replacement for the passive, planar DMFC, which is currently aggressively investigated.

1.3. Literature Review

1.3.1. Experimental Work

There have been very few experimental [5-14] and numerical [15] research efforts on tubular-shaped DMFCs. Considering the experimental work conducted on the tubular-shaped DMFCs, the main challenge has been to construct the fuel cell in such a way that prevents leaks and reduces the internal resistance. Kunimatsu and Okada [5] developed a semi-passive (active anode and passive cathode), tubular DMFC operating with 1 M methanol solution that produced 12 mW cm^{-2} with methanol pumped through the anode channel at 1 ml hr^{-1}. They found that the catalyst layer composition and hot-pressing process were crucial to improving the performance of tubular-shaped DMFCs. Qiao et al. [6] used a wet-chemical deposition process to coat the anode catalyst layer onto a tubular membrane made from Flemion tubing. During half-cell testing, the micro-tubular DMFC produced 1.8 mW cm^{-2} with a 2.8 mg cm^{-2} anode catalyst loading. Qiao et al. [7] further developed a method to coat the catalyst onto the membrane of a tubular DMFC by using an impregnation reduction method. They [8] also created a process by which the chemical reduction of Pt could be used to deposit a cathode catalyst layer onto the tubular membrane of a DMFC. They were able to carefully control the loading and thickness of the catalyst layer.

Shao et al. [9,10] built a tubular DMFC with a Titanium mesh current collector at the anode and cathode. They developed a method of dipping the Titanium mesh into different solutions until desired loads of Nafion® layers, catalyst layers, and Gas Diffusion Layers (GDL) were achieved. They explained this procedure and its results during half cell testing of the anode and cathode. M.S. Yazici [11] developed a tubular

fuel cell that could operate with Hydrogen or Methanol at the anode and used a material called GRAFCELL® (porous graphite material) as the GDL to control the fuel flow rate to each catalyst layer. Different open-hole ratios of graphite GDL material were investigated and it was concluded that water and air management at the cathode, as well as, liquid fuel management at the anode could be accomplished with different pore sizes and thinner GDLs.

Yu et al. [12] developed a semi-passive tubular DMFC that produced 10 mW cm^{-2} with 4 M methanol solution flowing through the anode at 80 ºC. Their DMFC included a new electrolyte membrane made from a porous silica pipe that had pores filled with perfluorinated resin and analyzed the membrane using a scanning electron microscope (SEM), electrochemical impedance spectroscopy system (EIS), and the bubble method to analyze the cross sections, conductivity, and porosity, respectively. Lee et al. [13] investigated the advantages of developing a tubular versus a planar DMFC including the overall specific power and volumetric energy density. They also constructed a tubular DMFC that consisted of 6 small planar DMFCs connected in a circular design that allowed passive anode and cathode operation that produced 12 mW cm^{-2} with 3 M methanol solution at room temperature.

Most recently, Ward et al. [14] designed and built a tubular-shaped fuel cell that operated completely passively. By constructing the fuel cell with a tubular-shaped frame, both Nafion® 212 and 115 membranes, and installing planar MEAs into the tubular frame, they were able to reduce the internal resistance below 50 mΩ. Their DMFC produced a maximum of 24.5 mW cm^{-2} with 3 M methanol and 19.4 mW cm^{-2} with 2 M methanol.

1.3.2. Numerical Work

Regarding the numerical efforts, Xu and Faghri [15] recently developed a two-dimensional, two-phase, non-isothermal model for an active, tubular, liquid-feed DMFC. Mass transport in the anode and cathode was based on the drift-flux and homogeneous mist-flow models, respectively. The model captured water and methanol crossover along with the effect of current density, methanol flow rate, and oxygen flow rate on the mass and heat transport characteristics. They also investigated the difference in energy density between active tubular and active planar DMFCs. Further expanding upon this work and described in detail in this thesis, Ward et al. [16] developed a two-dimensional, two-phase, non-isothermal model to investigate the steady-state performance and design characteristics of a tubular-shaped, passive DMFC. They found that increasing the ambient temperature increases the power density produced by the fuel cell, but that the thickness of the Cathode Transport Layer (CTL) significantly affected performance by restricting Oxygen transport to the cathode catalyst layer.

1.3.3. Discussion

From the experimental review, it was concluded that there was a lot of unresolved issues concerning the tubular-shaped DMFC. Considering each of the works described above, the successful and unsuccessful approaches to building the fuel cell were noted and examined during construction of a new tubular-shaped fuel cell. One of the major factors not considered in previous work, was designing and fabricating a frame to house the tubular MEA in order to prevent liquid fuel leaks and to apply sufficient pressure across the MEA layers in an attempt to significantly reduce the internal resistance. This form of resistance was noted several times in previous works as a major contributor towards the poor performance of each fuel cell. Another factor that was considered

during the design stages was the potential to operate the tubular-shaped DMFC actively, semi-passively, and also passively so that different testing modes could be used to examine several aspects of the fuel cell. Active operation presented an opportunity to produce the optimum results while semi-passive testing provided methods for examining the water crossover and water content in the membrane. Ultimately, the goal is to operate the fuel cell passively, so several designs were discussed that allowed passive air flow to the outer cathode portion of the MEA while also providing sufficient compression across the MEA. One final note is that Nafion® membranes were used as the central polymer electrolyte membrane to increase proton conductivity and produce comparable results to the existing planar-shaped, passive DMFC.

References

[1] Larminie, J., Dicks, A., 2000, Fuel Cell Systems Explained, John Wiley & Sons Ltd, New York, NY.

[2] Spiegel, C.S., 2007, Designing & Building Fuel Cells, McGraw Hill, New York, NY.

[3] Chu D, Jiang R. Effect of Operating Conditions on Energy Efficiency for a Small Passive Direct Methanol Fuel Cell. Electrochimica Acta 2006;51:5829-35.

[4] Maher A.R., Sadiq A.B. Three-Dimensional Computational Fluid Dynamics Model of a Tubular-Shaped PEM Fuel Cell. Renewable Energy 2008;33:1334-45.

[5] Kunimatsu M, Okada T. Performance of Microtubular DMFCs. Electrochemical and Solid-State Letters 2004;7:A389-90.

[6] Qiao H, Kasajima T, Kunimatsu M, Fujiwara N, Okada T. Evaluation of a Passive Microtubular Direct Methanol Fuel Cell with PtRu Anode Catalyst Layers Made by Wet Chemical Processes. Journal of the Electrochemical Society 2006;153:A42-7.

[7] Qiao H, Kunimatsu M, Fujiwara N, Okada T. Novel Heat-Treatment Process for Performance Enhancement of a Microtubular DMFC Anode Prepared by Impregnation-Reduction Method. Electrochemical and Solid-State Letters 2005;8:A175-8.

[8] Qiao H, Kunimatsu M, Okada T. Pt catalyst configuration by a new plating process for a micro tubular DMFC cathode. Journal of Power Sources 2005;139:30-4.

[9] Shao ZG, Lin WF, Zhu F, Christensen PA, Zhang H, Yi B. A tubular direct methanol fuel cell with Ti mesh anode. Journal of Power Sources 2006;160:1003-8.

[10] Shao ZG, Lin WF, Zhu F, Christensen PA, Zhang H. Tubular Cathode Prepared by a Dip-Coating Method for Low Temperature DMFC. Fuel Cells 2006;6:326-30.

[11] Yazici MS. Passive air management for cylindrical cartridge fuel cells. Journal of Power Sources 2007;166:137-42.

[12] Yu RJ, Cao GY, Liu XQ, Li ZF, Xing W, Zhu XJ. Fabrication of Support Tubular Proton Exchange Membrane For Fuel Cell. Journal of Fuel Cell Science and Technology 2007;4:520-4.

[13] Lee M, Chen L, Hung M, Lo M, Sue S, Lo C, et al. A Novel Design of a Cylindrical Portable Direct Methanol Fuel Cell. Journal of Fuel Cell Science and Technology 2008;5:1-8.

[14] Ward T, Li X, Faghri A. Performance Characteristics of a Novel Tubular-Shaped Direct Methanol Fuel Cell. Journal of Power Sources 2011;196:6264-73.

[15] Xu C, Faghri A. Analysis of an active tubular liquid-feed direct methanol fuel cell. Journal of Power Sources 2011;196:6332-46.

[16] Ward T, Xu C, Faghri A. Performance and design analysis of tubular-shaped passive direct methanol fuel cells. The International Journal of Hydrogen Energy 2011; 36:9216-30.

Chapter 2. Performance and design analysis of tubular-shaped passive direct methanol fuel cells

2.1. Background

The goal of this project is to explore the potential applications of passive, tubular-shaped DMFCs. There have not been any numerical simulations of passive tubular-shaped DMFCs represented in the literature. As a result, a two-dimensional, two-phase, non-isothermal numerical model was developed to investigate the steady-state performance and optimum design characteristics of a tubular shaped, liquid-feed, DMFC operating completely passively. Both 20 and 40 ºC ambient temperatures, various inlet methanol concentrations ranging from 1 to 3 M, and different Cathode Transport Layer (CTL) thicknesses from 1.0 to 10.0 mm were investigated to see their effects on the overall performance of the tubular DMFC. This work is published in the International Journal of Hydrogen Energy [1].

2.2. Optimization of VPD

This section will include an investigation of the instantaneous power produced versus the total volume occupied, VPD, for both tubular and planar, passive DMFCs. In this work, VPD is defined as the ratio of the instantaneous power produced by an electronic power source to the total volume occupied by the electronic power source. First, a detailed explanation of the tubular and planar DMFC stack designs is provided followed by a description of how the instantaneous power and volume from each stack design is calculated. All assumptions made during the analysis are presented and finally a comparison of the maximum VPD from each design, considering two different cases, is shown. Figure 2.1 presents a schematic of a passive, tubular DMFC including the tubular geometry terms.

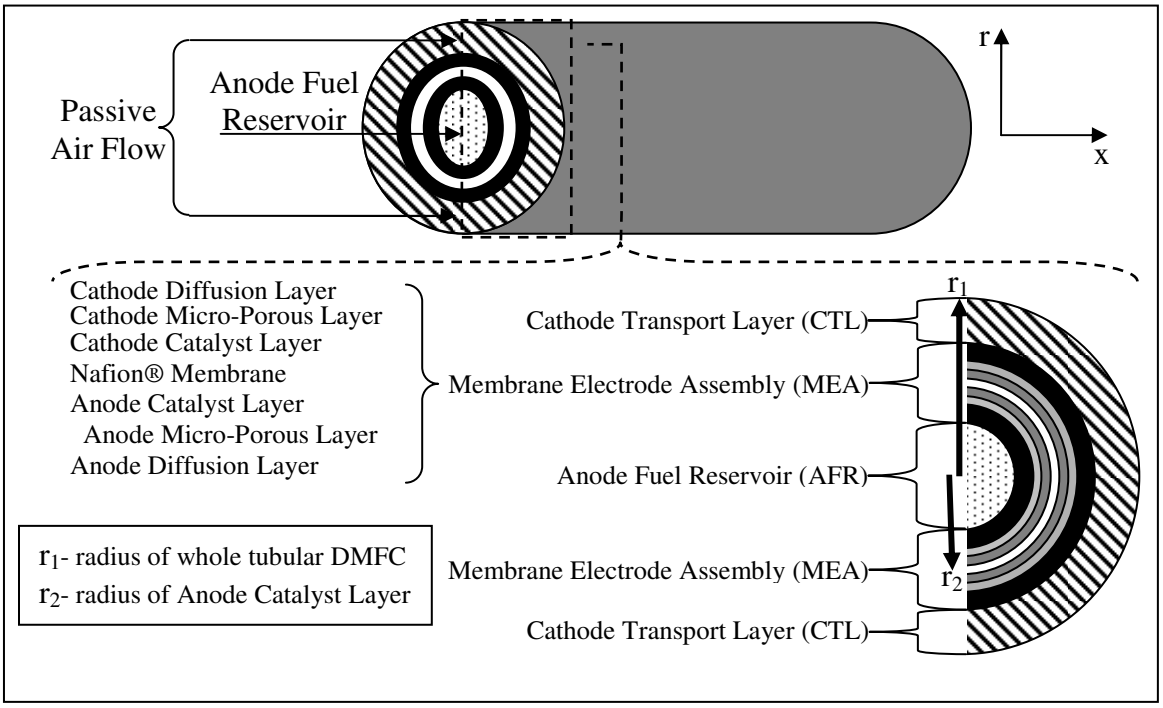

Figure 2.1: Tubular, Passive DMFC Schematic.

The present comparison of tubular versus planar DMFCs is different from the analysis performed by Xu and Faghri [2], because the present analysis considers:

- The thickness of the Anode Fuel Reservoir (AFR) and CTL to be variables that are changed in order to produce the highest ratio of tubular to planar VPD.
- A stack of four tubular DMFCs and a stack of four planar DMFCs when calculating the total power produced and volume occupied.
- Totally passive stacks of both tubular and planar DMFCs.

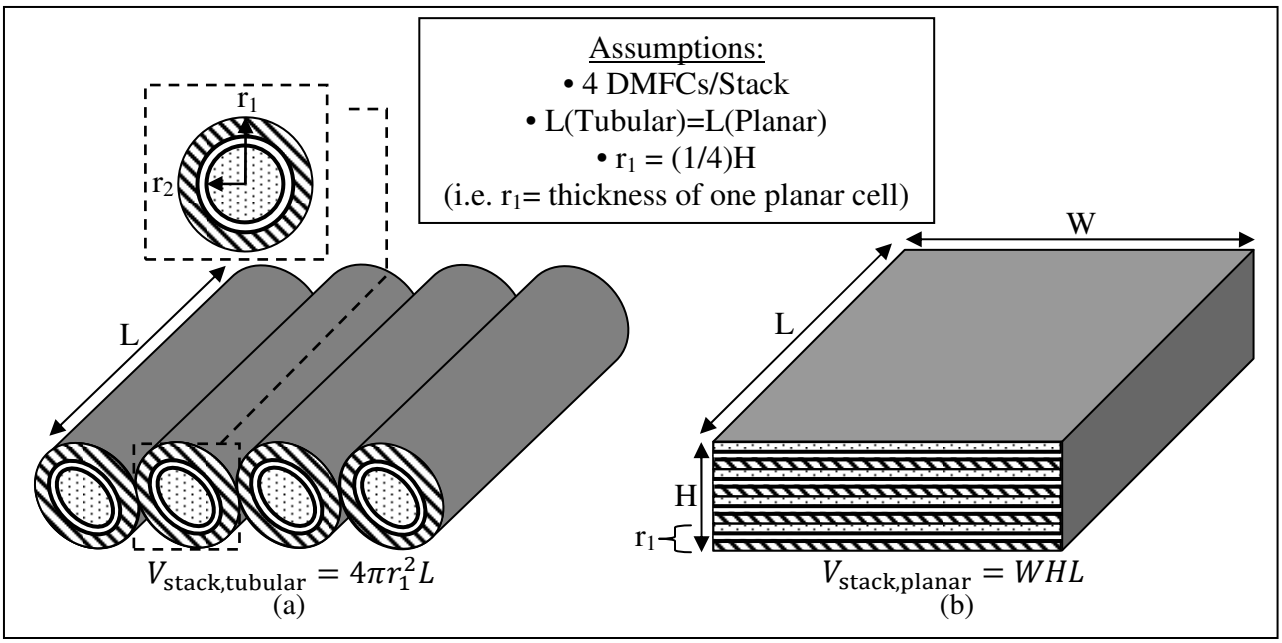

Figure 2.2: Passive DMFC Stacks (a) Tubular and (b) Planar.

Figure 2.2 provides a visual description of two geometrically different, completely passive DMFC designs. Figure 2.2(a) shows a stack of tubular-shaped, passive, DMFCs with the anode positioned on the inside of the tubular DMFC and the cathode positioned on the outside. Figure 2.2(b) shows a stack of planar-shaped, passive DMFCs. Each of the four planar DMFCs has an AFR positioned at the top of the cell, followed by an MEA below the AFR, and finally a CTL below the MEA to allow the transport of air to the CCLs.

For a single passive DMFC, the maximum voltage is about 0.6-0.7 V, which is far too low, even for most portable, low power applications (cell phones, PDAs, IPods~3.6 V). As a result, in order to produce a power supply with a desirable voltage range, several fuel cells are connected together in series resulting in a total output voltage equal to the sum of all the individual cell voltages On the other hand, in order to increase the overall current produced by the fuel cell stack, the cells must be connected in parallel. Based on the power constraints required from the specific application of the DMFC stack, parallel, series, or both configurations can be constructed to meet the specific power consumption of the device. It should also be noted that due to the non-linear nature of the performance curves produced by a DMFC, that a DC-DC conversion stage must be implemented in real applications to assure a constant, steady output voltage.

The instantaneous power produced by a stack of DMFCs in series configuration is:

$$\boldsymbol{P_{\text{stack}} = V_{\text{cell}} I_{\text{density}} (4A)} \quad (1)$$

where V_{cell} is the cell voltage, I_{density} is the current density produced by the fuel cell, and A is the area of the active surface at the anode. The active area for the tubular and planar DMFCs is:

$$\boldsymbol{A_{\text{tubular}} = 2\pi r_2 L} \tag{2}$$

and

$$\boldsymbol{A_{\text{planar}} = WL} \tag{3}$$

where L is the characteristic length of both the tubular and planar DMFC stacks, r_2 is the radius to the ACL shown in Figs. 2.1 and 2.2(a), and W is the characteristic width of the planar DMFC stack. Both stacks consist of four passive DMFCs and the total volume of each stack is represented as:

$$V_{\text{tubular}} = 4\pi r_1^2 L \tag{4}$$

and

$$V_{\text{planar}} = WHL \tag{5}$$

where r_1 is the radius of the entire tubular DMFC shown in figs. 2.1 and 2.2(a). Assumptions made for this analysis include:

- Porous, metal current collectors at the anode and cathode are neglected
- Both planar and tubular stacks are connected in series configurations
- L(Tubular)=L(Planar)
- The Planar and Tubular DMFCs both produce the same voltage and current density (valid if both cells are composed of the same MEA, operated with the same methanol concentration, and have equal pressure across the MEA)
- $r_1 = \left(\frac{1}{4}\right) H$, since the planar stack contains 4 DMFCs and r_1 is the thickness of one DMFC

- Each stack contains exactly 4 cells

The ratio of the VPD for the tubular stack to the VPD for the planar stack is:

$$\frac{\left(\frac{P_{\text{tubular}}}{V_{\text{tubular}}}\right)}{\left(\frac{P_{\text{planar}}}{V_{\text{planar}}}\right)} = \frac{\left(\frac{V_{\text{cell}} I_{\text{density}} (4A_{\text{tubular}})}{4\pi r_1^2 L}\right)}{\left(\frac{V_{\text{cell}} I_{\text{density}} (4A_{\text{planar}})}{WHL}\right)} = \frac{\left(\frac{2\pi r_2 L}{4\pi r_1^2 L}\right)}{\left(\frac{WL}{W(4r_1)L}\right)} = \frac{2r_2}{r_1} \quad (6)$$

The thickness of the CTL (YCTL) and the thickness of the AFR (YAFR) remain variables in order to find the optimum thicknesses for both layers that produce the highest tubular to planar VPD ratio. It should be noted that the tubular DMFC, which has a higher VPD than the planar DMFC for certain geometric conditions, would be beneficial for small-scale, portable applications that require large power output from an electronic power source.

In the next section, the performance of the passive, tubular DMFC for different CTL thicknesses (1 to 5, and 10 mm) is numerically investigated in order to obtain a minimum CTL thickness that would allow sufficient oxygen transport across the entire length of the cathode side of the fuel cell.

2.3. Model description

A steady-state, two-dimensional, two-phase, non-isothermal, mass transport model was developed. The effects of the geometric dimensions, methanol concentrations, and ambient temperatures are investigated in order to obtain an optimum performance for a completely passive, tubular-shaped DMFC. The following assumptions are made:

i. The porous layers are homogenous and isotropic.

ii. Both the gas and liquid phases are continuous throughout the porous layers.

iii. The only condensable species are water and methanol.

iv. The gas and liquid phases are assumed to be at the same temperature.

v. The polymer electrolyte membrane separating the anode and cathode sides of the fuel cell acts as an insulator that is impermeable to liquid and gas. Methanol and water do crossover the membrane through a “dissolved” phase only.

vi. The CTL is considered as a porous region and Darcy’s Law is used through all the porous regions.

vii. The model is axi-symmetric as is shown in Fig. 2.3.

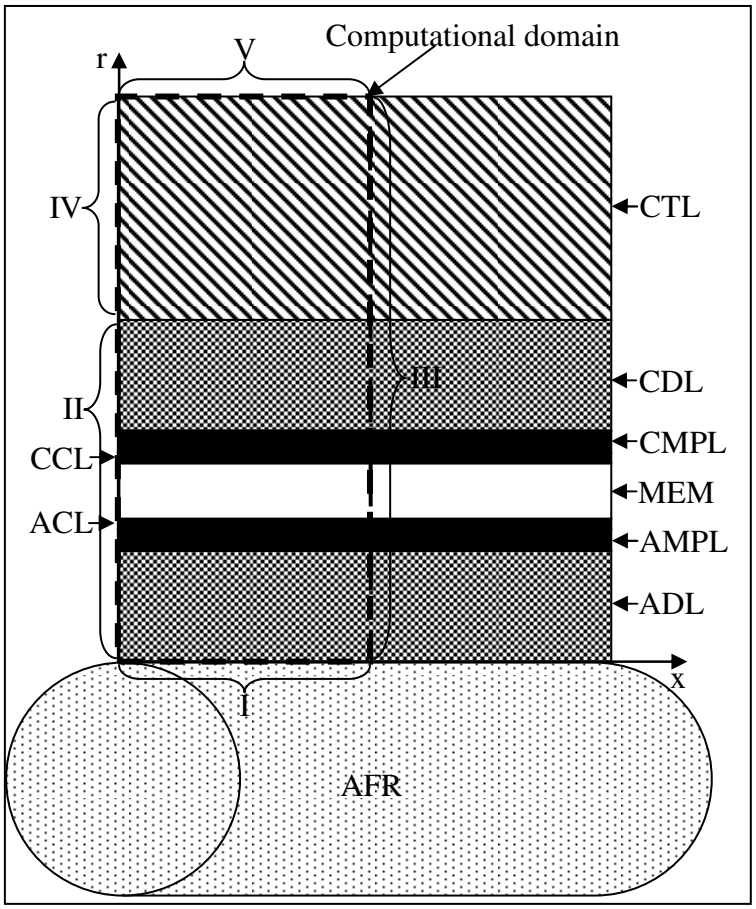

Figure 2.3: Tubular DMFC Computational Domain.

The two phases described by this model are liquid and gas. They both exist in all porous layers and the model accounts for continuous phase change as a function of the capillary pressure and temperature. The model accounts for the transport of gaseous species (methanol, water vapor, and oxygen), liquid species (methanol and water), energy (as heat), and dissolved water and methanol across the membrane. Water and methanol are assumed to exist and be exchanged among three phases: liquid, dissolved, and vapor; these three phases are assumed to be in equilibrium for all species.

2.3.1. Computational domain

The full computational domain is shown in Fig. 2.3 surrounded by a dotted line with each individual layer labeled with respect to an x-r axes. The layers, from top to bottom, are the CTL, Cathode Diffusion Layer (CDL), Cathode Micro-Porous Layer (CMPL), CCL, Nafion® 115 Polymer Electrolyte Membrane (MEM), ACL, AMPL, and ADL. The AFR is also shown in Fig. 2.3 as a visual reference, but is not included in the computational domain. The cell geometric parameters, including the grid sizes and dimensions, are included in Table 2.1.

Table 2.1: Cell Geometric Parameters

Parameter		Symbol	Value	Unit	Reference
Dimensions:	ADL	YADL	$2.6x10^{-4}$	m	[14]
	AMPL	YAMPL	$0.3x10^{-4}$	m	[14]
	ACL	YACL	$0.2x10^{-4}$	m	[14]
	MEM	YMEM	$1.25x10^{-4}$	m	[14]
	CCL	YCCL	$0.2x10^{-4}$	m	[14]
	CMPL	YCMPL	$0.3x10^{-4}$	m	[14]
	CDL	YCDL	$2.6x10^{-4}$	m	[14]
	CTL	YCTL	$1.0\text{-}10.0x10^{-3}$	m	-
Length of Tubular DMFC		L	0.05	m	-
Grid:	x-	-	15	-	-
Direction					
	r-	-	143	-	-
Direction					

2.4. Model formulation

2.4.1. Porous regions

The anode section of the computational domain consists of the ACL, AMPL, and ADL. The cathode section of the computational domain consists of the CTL, CDL, CMPL, and CCL. All these layers are considered to be porous diffusion layers, each with their own unique properties found in Table 2.2 and in previous work from the authors [3]. Since this model describes a completely passive DMFC, there is no anode fuel channel. For simplicity in numerical coding, the CTL is also modeled as a porous layer with a high porosity, i.e., the full Navier-Stokes equation was not solved for this region.

Table 2.2: Physicochemical Properties Not Listed in [3]

Parameter	Symbol	Value	Unit
Porosity, Permeability: CTL	ε_{ctl},K_{ctl}	0.99, 1.0×10^{-12}	-, m^2
Thermal Conductivity: CTL	k_{CTL}	0.024	$W\ m^{-1}K^{-1}$

Both liquid and gas flow are considered in the porous layers. The mass balance equations for the liquid and gas flow in the anode or cathode are [2-7]:

$$\text{Liquid Phase: } \nabla \cdot (\rho_l \vec{u}_{\mathrm{l,a/c}}) = \dot{m}_{\mathrm{l,a/c}} \tag{7}$$

and

$$\text{Gas Phase: } \nabla \cdot (\rho_{\mathrm{g}} \vec{u}_{\mathrm{g,a/c}}) = \dot{m}_{\mathrm{g,a/c}} \tag{8}$$

where ρ_{l} is the average density of the liquid, ρ_{g} is the average density of the gas, $\vec{u}_{\mathrm{l,a/c}}$ is the average liquid velocity in the anode/cathode porous media, $\vec{u}_{\mathrm{g,a/c}}$ is the average gas velocity in the anode/cathode porous media, $\dot{m}_{\mathrm{l,a/c}}$ is the rate of liquid generation in the anode/cathode, and $\dot{m}_{\mathrm{g,a/c}}$ is the rate of gas generation in the anode/cathode.

Applying initial assumptions made previously and assuming no viscous, body or inertial terms, the momentum equations for both the liquid and gas phases reduce to Darcy's Law. Darcy's Law is dependent on the relative permeability of each phase, which is related to the reduction in total cross-sectional area in each pore of the porous media due to the presence of the second phase. The following equations represent the momentum conservation for the liquid and gas phases in the anode or cathode:

$$\text{Liquid Phase: } \vec{u}_{\mathrm{l,a/c}} = -K \frac{K_{\mathrm{rl}}}{\mu_{\mathrm{l}}} \nabla P_{\mathrm{l,a/c}} \tag{9}$$

and

$$\text{Gas Phase: } \vec{u}_{\mathrm{g,a/c}} = -K \frac{K_{\mathrm{rg}}}{\mu_{\mathrm{g}}} \nabla P_{\mathrm{g,a/c}} \tag{10}$$

where K is the relative permeability of the porous media, K_{rl} is the relative permeability of the liquid phase, K_{rg} is the relative permeability of the gas phase, μ_l is the viscosity of the liquid phase, μ_{g} is the viscosity of the gas phase, $P_{\mathrm{l,a/c}}$ is the anode/cathode liquid pressure, and $P_{\mathrm{g,a/c}}$ is the anode/cathode gas pressure.

There are five different species (liquid methanol, methanol vapor, liquid water, water vapor, and carbon dioxide gas) calculated in the anode side of the DMFC and there are three different species (liquid water, water vapor, and oxygen gas) calculated in the cathode side of the DMFC. It is assumed that all the crossover liquid methanol immediately reacts in the CCL, leaving no methanol (liquid or vapor) present in the cathode side. Taking into account the assumptions previously stated, the general form of the species conservation equation is:

$$\nabla \cdot \left(\vec{u}_{\mathrm{i,a/c}} C_{\mathrm{k,i,a/c}}\right) = \nabla \cdot \left(D^{\mathrm{eff}}_{\mathrm{k,i,a/c}} \cdot \nabla C_{\mathrm{k,i,a/c}}\right) + \dot{R}_{\mathrm{k,i,a/c}} \tag{11}$$

where i=phase and k=species, $D^{\mathrm{eff}}_{\mathrm{k,i,a/c}}$ is the effective diffusivity of species k in the anode/cathode, and $\dot{R}_{\mathrm{k,i,a/c}}$ is the mass generation rate of species k in the anode/cathode.

2.4.2. Membrane

For this model, the membrane is considered to be Nafion® 115, a popular membrane material used in both numerical and experimental analyses of PEMFCs and DMFCs. Since the membrane does not allow liquid or gas species to penetrate, water and methanol can only crossover through a dissolved phase. Water crossover is due to three phenomena: diffusion, electro-osmotic drag, and convection. Hence the molar flux of water crossover through the membrane can be given by [3]:

$$N_{\mathrm{W,cr}} = -D_{\mathrm{W,N}}(\lambda)\nabla C_{\mathrm{we}} + n_{\mathrm{d,W}}\frac{I}{F} - \frac{K_{\mathrm{mem}}\rho_{\mathrm{dry}}}{\mu_{\mathrm{l}} M_{\mathrm{W}}}\nabla P_{\mathrm{l}} \tag{12}$$

where $N_{\mathrm{W,cr}}$ is the molar flux of water crossover, $D_{\mathrm{W,N}}$ is the dissolved water diffusivity coefficient, $n_{\mathrm{d,W}}$ is the electro-osmotic drag coefficient for water, I is the current density applied across the fuel cell, F if Faraday's constant, ρ_{dry} is the density of the dry Nafion® 115 membrane, K_{mem} is the permeability of the Nafion® 115 membrane, and

M_{W} is the molecular weight of water. Similarly, the methanol crossover is also due to diffusion, electro-osmotic drag, and convection. The molar flux of methanol crossover can be given by [3]:

$$N_{\mathrm{M,cr}} = -D_{\mathrm{M,N}} \nabla C_{\mathrm{M,l}} + n_{\mathrm{d,M}} \frac{I}{F} - \left(\frac{K_{\mathrm{mem}} \Delta P_{\mathrm{l,c-a}}}{\mu_{\mathrm{l}}(\mathrm{YMEM})} \right) C_{\mathrm{M,l}} \tag{13}$$

where $N_{\mathrm{M,cr}}$ is the molar flux of methanol crossover, $\mathrm{D_{M,N}}$ is the diffusivity of methanol in Nafion®, $n_{\mathrm{d,M}}$ is the electro-osmotic drag coefficient for methanol, $\Delta P_{\mathrm{l,c-a}}$ is the change in liquid pressure between the cathode and anode, and YMEM is the thickness of the membrane.

2.4.3. Energy transport

The simplified energy equation is used to model the non-isothermal temperature changes through the entire computational domain. The temperature of the entire DMFC is initially set to ambient levels, which include 20 and 40 ℃ to account for changes in the ambient temperature depending on where the DMFC is operated. All the heat produced from the fuel cell is dissipated away from the fuel cell to the ambient air through the CTL entrance/ exit, since the walls of the fuel cell are considered adiabatic. Heat is generated in the fuel cell due to different mechanisms in each layer:

- ADL, AMPL- Latent heat of phase change of water and methanol
- ACL- Latent heat of phase change of water and methanol, electrochemical reactions, and Joule heat
- MEM- Joule heat
- CCL- Latent heat of phase change of water, electrochemical reactions, and Joule heat
- CDL, CMPL- Latent heat of phase change of water

The latent heat of phase change of water and methanol is associated with the heat that is either absorbed or released during phase change of the water and methanol between liquid and gas. The heat generation from the anode electrochemical reaction is due to activation and mass transport over-potentials as well as the entropy change due to the Methanol Oxidation Reaction (MOR). The heat generation from the cathode electrochemical reactions is due to activation and mass transport over-potentials, mixed potential from the methanol crossover, entropy change from the Oxygen Reduction Reaction (ORR), and the entropy change due to the MOR at the CCL.

2.4.4. Boundary conditions

Boundary conditions are provided for all outer sides of the computational domain. Each individual boundary condition is also labeled in Fig. 2.3.

Boundary I: This is the boundary between the AFR and the ADL. The supply of methanol solution in the AFR is considered to be large enough, such that it will not be affected by the consumption of methanol at the ACL, i.e. the concentration of methanol at this surface is considered to be a constant during all operation.

$$C_{\mathrm{M,l}} = C_{\mathrm{M,l\ tank}} \tag{14}$$

$$C_{\mathrm{M,g}} = C_{\mathrm{M,g}}^{\mathrm{sat}} \tag{15}$$

$$C_{\mathrm{W,g}} = C_{\mathrm{W,g}}^{\mathrm{sat}} \tag{16}$$

$$P_{\mathrm{l,a}} = P_{\mathrm{l,a\ tank}} \tag{17}$$

$$P_{\mathrm{g,a}} = P_{\mathrm{l,a\ tank}} + P_{\mathrm{c}}(s) \tag{18}$$

$$s = .95 \tag{19}$$

Boundary II: This boundary represents the exterior wall of the fuel cell/MEA which is facing the ambient air and excludes the CTL external surface. This surface is adiabatic and insulated from the ambient air surrounding the fuel cell. There is no transport of any species across this boundary.

For the ADL, AMPL, and ACL layers:

$$\frac{\partial \Phi}{\partial x} = 0 \text{ where } \Phi = C_{\mathrm{M,l}}, C_{\mathrm{M,g}}, C_{\mathrm{W,l}}, C_{\mathrm{W,g}}, P_{\mathrm{l,a}}, P_{\mathrm{g,a}}, T \tag{20}$$

For the MEM layer:

$$\frac{\partial \Phi}{\partial x} = 0 \text{ where } \Phi = \lambda \; and \; T \tag{21}$$

For the CCL, CMPL, and CDL layers:

$$\frac{\partial \Phi}{\partial x} = 0 \text{ where } \Phi = C_{\mathrm{M,l}}, C_{\mathrm{W,l}}, C_{\mathrm{W,g}}, C_{\mathrm{O_2,g}}, P_{\mathrm{l,c}}, P_{\mathrm{g,c}}, T \tag{22}$$

Boundary III: This is a symmetrical boundary. In order to reduce the overall computational time, the entire computational domain is cut in half parallel to the r-axis, thus it is identical on both sides of the dotted line shown in Fig. 2.3. There is no flux of any species across this boundary. Unlike Boundary II, this boundary includes the CTL.

For the ADL, AMPL, and ACL layers:

$$\frac{\partial \Phi}{\partial x} = 0 \text{ where } \Phi = C_{\mathrm{M,l}}, C_{\mathrm{M,g}}, C_{\mathrm{W,l}}, C_{\mathrm{W,g}}, P_{\mathrm{l,a}}, P_{\mathrm{g,a}}, T \tag{23}$$

For the MEM layer:

$$\frac{\partial \Phi}{\partial x} = 0 \text{ where } \Phi = \lambda \; and \; T \tag{24}$$

For the CCL, CMPL, and CDL layers:

$$\frac{\partial \Phi}{\partial x} = 0 \text{ where } \Phi = C_{\mathrm{M,l}}, C_{\mathrm{W,l}}, C_{\mathrm{W,g}}, C_{\mathrm{O_2,g}}, P_{\mathrm{l,c}}, P_{\mathrm{g,c}}, T \tag{25}$$

For the CTL layer:

$$\frac{\partial \Phi}{\partial x} = 0 \text{ where } \Phi = C_{\mathrm{W,g}}, C_{\mathrm{O_2,g}}, P_{\mathrm{g,c}}, T \tag{26}$$

Boundary IV: This boundary represents the exterior entrance of the CTL, which allows ambient air to the CDL. Water vapor and heat are also removed from the fuel cell through the CTL.

$$P_{\mathrm{g,c}} = P_{\mathrm{g,c}}^{\infty} \tag{27}$$

$$-D_{\mathrm{O_2,g,c}}^{\mathrm{eff}} \frac{\partial C_{\mathrm{O_2,g,c}}}{\partial x}\Big|_{\_} = h_{\mathrm{m}}\left(C_{\mathrm{O_2,g,c}} - C_{\mathrm{O_2,g,\infty}}\right) \tag{28}$$

$$-D_{\mathrm{W,g,c}}^{\mathrm{eff}} \frac{\partial C_{\mathrm{W,g,c}}}{\partial x}\Big|_{\_} = h_{\mathrm{m}}\left(C_{\mathrm{W,g,c}} - C_{\mathrm{W,g,\infty}}\right) \tag{29}$$

$$-K_{\mathrm{T}}^{\mathrm{eff}} \frac{\partial T}{\partial x}\Big|_{\_} = h(T - T_{\infty}) \tag{30}$$

The heat and mass transfer correlations for a horizontal surface pointing down were used to find h and h_{m} as [7]:

$$\overline{Nu} = \frac{\bar{h}(YCFTL)}{K} = .27(GrPr)^{.25}, Gr = \frac{g\beta|\Delta T|(YCFTL)^3}{\nu^2}, Pr = \frac{\nu}{\alpha} \tag{31}$$

$$\overline{Sh} = \frac{\bar{h}_{\mathrm{m}}(YCFTL)}{D_{\mathrm{O_2,g}}} = .27(GrSc)^{.25}, Gr = \frac{g\rho|\Delta\rho|(YCFTL)^3}{\mu^2}, Sc = \frac{\nu}{D_{\mathrm{O_2,g}}} \tag{32}$$

Boundary V: This boundary represents the top of the CTL. In this model, the top of the CTL is considered to be a no-flux wall, but in a real application the top of the CTL would either be the edge of a CTL from a neighboring tubular DMFC or the external casing surrounding the stack of tubular DMFCs, as shown in Fig. 2.1. One goal of this model is to find the minimum thickness of the CTL that would not result in a lack of oxygen being available to any location along the length of the CCL. Thus, by implementing a no-flux boundary at the top of the CTL, the only source of oxygen to the CTL is through Boundary IV, either end of the tubular DMFC. There is no flux of any species across Boundary V.

$$\frac{\partial \Phi}{\partial r} = 0 \text{ where } \Phi = C_{\mathrm{W,g}}, C_{\mathrm{O_2,g}}, P_{\mathrm{l,c}}, P_{\mathrm{g,c}} \tag{33}$$

2.4.5. Interface conditions

ACL/MEM Interface: The specific conditions at this interface must be provided, because there are discontinuities in the species concentrations and pressure gradients across the MEM layer. To account for both methanol and water crossovers, the dissolving of liquid methanol and liquid water into the membrane is considered to be a source term that takes place completely in the ACL.

$$\left.\frac{\partial \phi}{\partial r}\right|_{-} = 0 \text{ for } \phi = C_{\mathrm{M,l,a}}, C_{\mathrm{M,g,a}}, C_{\mathrm{W,g,a}}, P_{\mathrm{l,a}}, P_{\mathrm{g,a}} \tag{34}$$

In addition, the concentration of dissolved water at the surface of the membrane is assumed to be in equilibrium with the water state in the porous ACL. The relationship between the concentration of dissolved water (C_{we}) in the ACL and the water content (λ) in the membrane is [3, 7]:

$$C_{\mathrm{we}} = \lambda \frac{\rho_{\mathrm{dry}}}{EW} \tag{35}$$

For a Nafion® membrane in equilibrium with saturated water vapor, the water content in the membrane approaches an equilibrium value based on the temperature [3, 7]:

$$\lambda_{\mathrm{g}}(T = 303) = .043 + 17.81a_{\mathrm{w}} - 39.85a_{\mathrm{w}}^2 + 36a_{\mathrm{w}}^3 \tag{36}$$

$$\lambda_{\mathrm{g}}(T = 353) = .3 + 10.8a_{\mathrm{w}} - 16a_{\mathrm{w}}^2 + 14.1a_{\mathrm{w}}^3 \tag{37}$$

where a_{w} is the water vapor activity expressed as [3, 7]:

$$a_{\mathrm{w}} = \frac{x_{\mathrm{g}} p_{\mathrm{g}}}{p_{\mathrm{g}}^{\mathrm{sat}}} \tag{38}$$

and the expression for the water content in equilibrium with water vapor at any temperature can be found by developing a linear approximation expression [3, 7]:

$$\lambda_{\mathrm{g}}(T) = \lambda_{\mathrm{g}}(T = 303) + \frac{\lambda_{\mathrm{g}}(T=353) - \lambda_{\mathrm{g}}(T=303)}{50}(T - 303) \tag{39}$$

For a Nafion® 115 membrane in equilibrium with saturated liquid water, $\lambda_{\mathrm{l}} = 22$. In order to find the equilibrium water content value for a two-phase, liquid-gas environment, a linear expression is used to approximate the overall water content value at the ACL/MEM interface based on the water content at the edge of the MEM as [3, 7]:

$$\lambda(T)|_{+} = \lambda_{\mathrm{g}}(T) + \left(\lambda_{\mathrm{l}} - \lambda_{\mathrm{g}}(T)\right) s|_{-} \tag{40}$$

CCL/MEM Interface: Similarly to the previous interface, the specific conditions at this interface must be provided as follows, because there are discontinuities in the species concentrations and pressure gradients across the Nafion® Membrane [3, 7].

$$\left.\frac{\partial \phi}{\partial r}\right|_{+} = 0 \text{ for } \phi = C_{\mathrm{O_2,g,c}}, C_{\mathrm{W,g,c}}, P_{\mathrm{l,c}}, P_{\mathrm{g,c}} \tag{41}$$

$$\lambda(T)|_{-} = \lambda_{\mathrm{g}}(T) + \left(\lambda_{\mathrm{l}} - \lambda_{\mathrm{g}}(T)\right) s|_{+} \tag{42}$$

2.4.6. Solution Procedure

In order to yield the Governing Equations (GE) for the liquid and gas pressures in the anode/cathode, equations (9) and (10) are substituted into equations (7) and (8), respectively:

$$\text{Anode/Cathode Liquid Phase GE: } \nabla \cdot \left(\rho_{\mathrm{l}} K \frac{K_{\mathrm{rl}}}{\mu_{\mathrm{l}}} \nabla P_{\mathrm{l,a/c}}\right) + \dot{m}_{\mathrm{l,a/c}} = 0 \tag{43}$$

$$\text{Anode/Cathode Gas Phase GE: } \nabla \cdot \left(\rho_{\mathrm{g}} K \frac{K_{\mathrm{rg}}}{\mu_{\mathrm{g}}} \nabla P_{\mathrm{g,a/c}}\right) + \dot{m}_{\mathrm{g,a/c}} = 0 \tag{44}$$

To derive the governing equation for the water content in the membrane, the dot product of the del operator and equation (15) is taken. Since the variable of interest in this governing equation, the water content in the membrane (λ), is only associated with the diffusive and electro-osmotic drag components of equation (15), all other components become zero:

Water Content GE: $\nabla \cdot \left(D_{\mathrm{W,N}} \frac{\rho_{\mathrm{dry}}}{EW} \cdot \nabla\lambda\right) - \nabla \cdot \left(n_{\mathrm{d,W}} \frac{I}{F}\right) = 0$ (45)

By simple rearrangement, the conservation equations for each species and energy become:

Anode Liquid Methanol GE: $\nabla \cdot \left(D^{\mathrm{eff}}_{\mathrm{M,l,a}} \cdot \nabla C_{\mathrm{M,l,a}}\right) - \nabla \cdot \left(u_{\mathrm{l}} C_{\mathrm{M,l,a}}\right) + \dot{R}_{\mathrm{M,l,a}} = 0$ (46)

Anode Methanol Vapor GE: $\nabla \cdot \left(D^{\mathrm{eff}}_{\mathrm{M,g,a}} \cdot \nabla C_{\mathrm{M,g,a}}\right) - \nabla \cdot \left(u_{\mathrm{g}} C_{\mathrm{M,g,a}}\right) + \dot{R}_{\mathrm{M,g,a}} = 0$ (47)

Anode Water Vapor GE: $\nabla \cdot \left(D^{\mathrm{eff}}_{\mathrm{W,g,a}} \cdot \nabla C_{\mathrm{W,g,a}}\right) - \nabla \cdot \left(u_{\mathrm{g}} C_{\mathrm{W,g,a}}\right) + \dot{R}_{\mathrm{W,g,a}} = 0$ (48)

Cathode Oxygen Gas DE: $\nabla \cdot \left(D^{\mathrm{eff}}_{\mathrm{O_2,g,c}} \cdot \nabla C_{\mathrm{O_2,g,c}}\right) - \nabla \cdot \left(u_{\mathrm{g}} C_{\mathrm{O_2,g,c}}\right) + \dot{R}_{\mathrm{O_2,g,c}} = 0$ (49)

Cathode Water Vapor GE: $\nabla \cdot \left(D^{\mathrm{eff}}_{\mathrm{W,g,c}} \cdot \nabla C_{\mathrm{W,g,c}}\right) - \nabla \cdot \left(u_{\mathrm{g}} C_{\mathrm{W,g,c}}\right) + \dot{R}_{\mathrm{W,g,c}} = 0$ (50)

Temperature GE: $\nabla \cdot \left(K^{\mathrm{eff}}_{\mathrm{T}} \cdot \nabla T\right) - \nabla \cdot \left(\rho_{\mathrm{l}} c_{\mathrm{pl}} \vec{u}_{\mathrm{l}} T + \rho_{\mathrm{g}} c_{\mathrm{pg}} \vec{u}_{\mathrm{g}} T\right) + S_{\mathrm{T}} = 0$ (51)

Constitutive relations can be found in previous work from the authors [3] and Appendix B provides a detailed description of all the source and effective diffusivity terms used to solve the governing equations.

The simulation-code, written to solve the governing equations and corresponding to the boundary and interface conditions was based on the SIMPLE algorithm using a finite-volume approach. The convergent criterions are a minimum variation of each parameter between successive iterations of 1.0 x 10^{-6}. It should also be noted that the methods used in this work to produce a numerical simulation of a two-dimensional, passive, tubular DMFC are based on previously well-developed models for passive DMFCs [2-7].

2.4.7. Liquid saturation

Liquid saturation, s, distinguishes the liquid volume fraction in a specified control volume. At the end of each iteration, the liquid saturation in each control volume is

calculated by using the popularly used Leverett function. The Leverett function develops a relationship between the liquid saturation and the capillary pressure, which is the difference between the gas and liquid pressure. The following equations describe the method of calculating the liquid saturation [2-7]:

$$P_{\mathrm{c}} = P_{\mathrm{g}} - P_{\mathrm{l}} \tag{52}$$

and

$$P_{\mathrm{c}} = [\sigma \cos(\theta)] \left(\frac{\varepsilon}{K}\right)^{.5} J(s) \tag{53}$$

where P_{c} is the capillary pressure, σ is the interfacial tension between the liquid and gas phases, θ is the contact angle caused by the hydrophobic/hydrophilic characteristics of the porous media, ε is the porosity of the porous media, K is the permeability of the porous media, and $J(s)$ is the Leverett function used to find the liquid saturation:

$$J(s) = \begin{cases} 1.417(1-s) - 2.120(1-s)^2 + 1.263(1-s)^3, & for\ 0 < \theta \leq 90^\circ \\ 1.417s - 2.120s^2 + 1.263s^2, & for\ 90^\circ < \theta < 180^\circ \end{cases} \tag{54}$$

2.4.8. Cell potential

The cell voltage is found by subtracting all irreversibilities from the thermodynamic, equilibrium voltage, V_0, of a DMFC, which is expressed as [5]:

$$V_{\mathrm{cell}} = V_0 - \eta_{\mathrm{a}} - \eta_{\mathrm{c}} - I(R_{\mathrm{contact}} + \frac{YMEM}{\sigma_{\mathrm{mem}}}) \tag{55}$$

where V_{cell} is the cell voltage, η_{a} is the anode overpotential, η_{c} is the cathode overpotential, I is the current applied to the cell, R_{contact} is the internal resistance across the Nafion® membrane, YMEM is the thickness of the Nafion® 115 membrane, and σ_{mem} is the proton conductivity of the membrane. R_{contact}, σ_{mem}, YMEM, and V_0 are constant values found elsewhere in [3], while η_{a} and η_{c} must be found by using the

Tafel-like expressions for both the anode and cathode kinetics. In the model, η_{a} is an initial condition parameter that is used to calculate η_{c}.

Initially, η_{a} is an inputted approximate value (0.2-0.6) that is used to find the anode current density, J_{a}, from:

$$J_{\mathrm{a}} = A_{\mathrm{v,a}} J_{\mathrm{o,M}}^{\mathrm{ref}} \left(\frac{C_{\mathrm{M,l}}}{C_{\mathrm{M}}^{\mathrm{ref}}}\right)^{\gamma} e^{\left(\frac{\alpha_{\mathrm{a}} F \eta_{\mathrm{a}}}{RT}\right)} \tag{56}$$

where $A_{\mathrm{v,a}} J_{\mathrm{o,M}}^{\mathrm{ref}}$ is the anode exchange current density, $C_{\mathrm{M}}^{\mathrm{ref}}$ is the reference concentration of methanol, γ is a reaction order constant, and α_{a} is the anode transfer coefficient. The anode current density is represented in terms of A m^{-3}, so in order to find the cell current density in terms of A m^{-2}, the anode current density is integrated by the total length of the fuel cell and divided by the length of the fuel cell to find the average cell current density:

$$I = \frac{1}{L} \int J_{\mathrm{a}} \, dx \tag{57}$$

Next, a similar procedure must be used to find the cathode current density, which is equal to, not only the cell current density, but also the parasitic current density due to methanol crossover and its reaction at the cathode by:

$$I_{\mathrm{p}} = 6F N_{\mathrm{M,cr}} \tag{58}$$

where $N_{\mathrm{M,cr}}$ is the total molar flux of methanol crossover represented by Eq. (13). The sum of the cell current density and parasitic current density are set equal to the integral of the cathode current density divided by the length of the fuel cell as:

$$I + I_{\mathrm{p}} = \frac{1}{L} \int J_{\mathrm{c}} \, dx \tag{59}$$

and the cathode current density is similarly calculated using the Tafel-like expression as:

$$J_{\mathrm{c}} = A_{\mathrm{v,c}} J_{\mathrm{o,O_2}}^{\mathrm{ref}} \left(\frac{C_{\mathrm{O_2,g}}}{C_{\mathrm{O_2}}^{\mathrm{ref}}}\right) e^{\left(\frac{\alpha_{\mathrm{c}} F \eta_{\mathrm{c}}}{RT}\right)} \tag{60}$$

where $A_{\mathrm{v,c}}J_{\mathrm{o,O_2}}^{\mathrm{ref}}$ is the cathode exchange current density, $C_{\mathrm{O_2}}^{\mathrm{ref}}$ is the reference concentration of oxygen, and α_{c} is the cathode transfer coefficient. From this expression, the cathode overpotential, η_{c}, is found and used to calculate the total cell voltage represented by Eq. (55).

2.5. Results and discussion

2.5.1. Instantaneous VPD

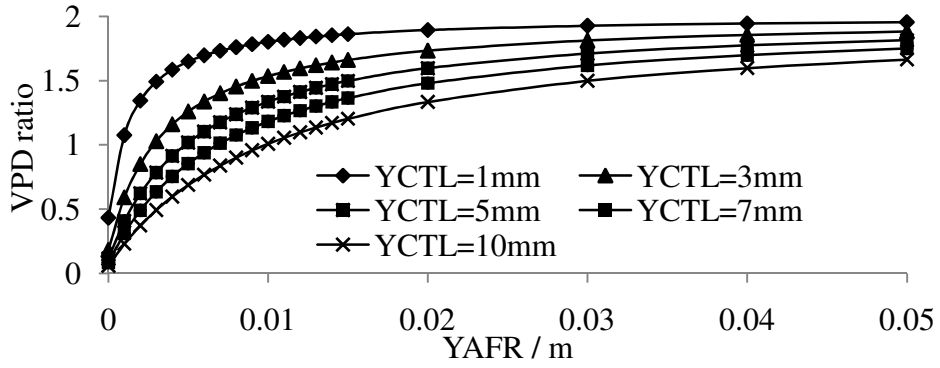

(a)

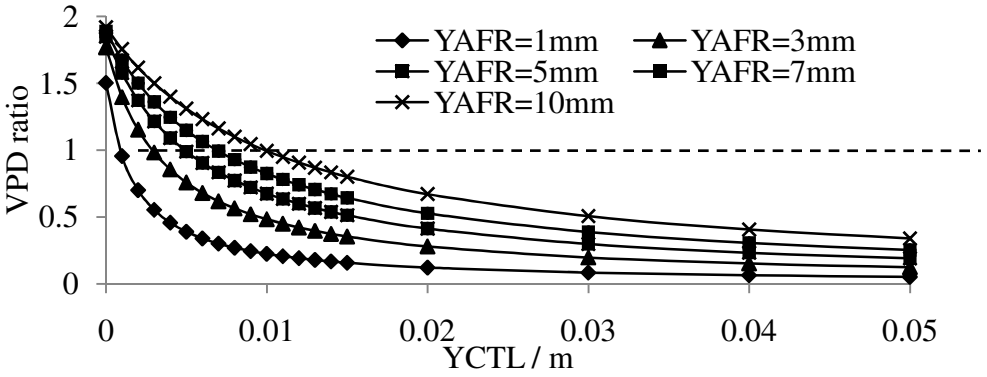

(b)

Figure 2.4: Ratio of Tubular to Planar VPD for (a) Constant CTL Thicknesses and Changing AFR Thicknesses and (b) Constant AFR Thickness and Changing CTL Thicknesses.

Considering the tubular to planar VPD ratio represented by Eq. (6), substituting values for the thickness of each layer in the fuel cell, listed in Table 2.1, and leaving YAFR and YCTL as variables for comparison, it is seen in Figs. 2.4(a) and (b) that by varying both YAFR and YCTL, that the ratio of the VPD of the tubular to the planar geometries varies between 0 and 2. In other words, the tubular stack has the capability of producing two times the instantaneous power of the planar stack considering both geometries occupy the same volume. For:

$0 < ratio < 1,$ Tubular VPD is **less** than Planar

$ratio = 1,$ Tubular and Planar VPDs are **equal**

$1 < ratio < 2,$ Tubular VPD is **more** than Planar

Figure 2.4(a) shows the change in the ratio of tubular to planar VPD for the case in which the YCTL remains a constant at 1, 3, 5, 7, and 10 mm. A range of YAFR values ranging from 0 to 50 mm are considered for each constant YCTL. It is shown that the ratio increases with an increase in YAFR for each constant YCTL. The smallest constant YCTL value, 1 mm, produces the highest ratio of tubular to planar VPD for all YAFR. For each constant YCTL, the VPD ratio increases from a minimum value to a maximum value as the YAFR increases from 0 to 50 mm. For each constant YCTL, the VPD ratio initially increases sharply for small YAFR, but approaches a horizontal asymptote (maximum) after the YAFR exceeds 20 mm. This means that for all YCTL, the maximum YAFR that produces the highest VPD ratio is less than or equal to 20 mm. Any YAFR larger than 20 mm produces a negligible difference in the VPD ratio, but does lead towards a larger overall stack volume which is unfavorable when considering potential

small, portable applications. In order to obtain a small overall stack volume, the optimum YAFR for this case is considered to be 10mm.

Figure 2.4(b) shows the change in the ratio of tubular to planar VPD while the YAFR remains a constant at 1, 3, 5, 7, and 10 mm. A range of YCTL values from 0 to 50 mm are considered for each constant YAFR. It is shown that the VPD ratio decreases as the YCTL increases for each constant YAFR. The goal is to produce the highest VPD ratio, so for a 10 mm thick AFR, only YCTL thicknesses from 1 to 10 mm in which the VPD ratio is greater or equal to 1.0 will be considered. For these cases, Fig. 2.4(b) shows that the 1 mm thick CTL would produce a VPD ratio of 1.96 and a 10 mm thick CTL would produce a VPD ratio of 1.0. This means that the tubular stack will produce 1.96 times the VPD of the planar stack for a 1 mm thick CTL and the tubular stack will produce the same VPD as the planar stack for a 10 mm thick CTL. In other words, the thinner CTL would ultimately be the best option since the tubular-shaped DMFC would produce the highest tubular to planar VPD ratio, and the 1 mm thick CTL would produce a tubular-shaped DMFC with a much smaller overall volume and more easily adaptable to small, portable applications.

Considering both Figs. 2.4(a) and (b), the optimum geometric conditions that would provide the highest ratio of tubular to planar VPD are for an AFR thickness of 10 mm and a CTL thickness less than or equal to 10 mm. These results were used during design stages of constructing a passive, tubular-shaped DMFC in order to prove that the tubular geometry would produce more power for a given volume compared to the planar geometry. One must also consider that a larger YCTL and YAFR together would result in optimum conditions for both tubular and planar passive DMFC stacks, because:

- A larger CTL thickness would allow easier passive oxygen transport to all points of the CCL along the length of the fuel cell.
- A larger AFR thickness would allow more methanol solution to be stored and thus result in longer runtime of the fuel cell.
- Comparatively, smaller YCTL and YAFR values would result in less overall cell and stack volume, thus, making it easier to fit more cells in a smaller stack volume and closing the gap in research towards producing DMFCs for portable electronic applications.

2.5.2. Effect of ambient air temperature

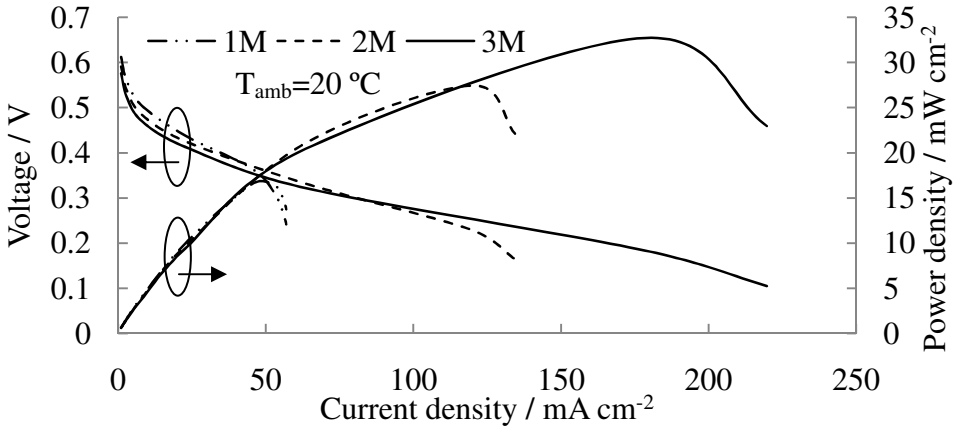

(a)

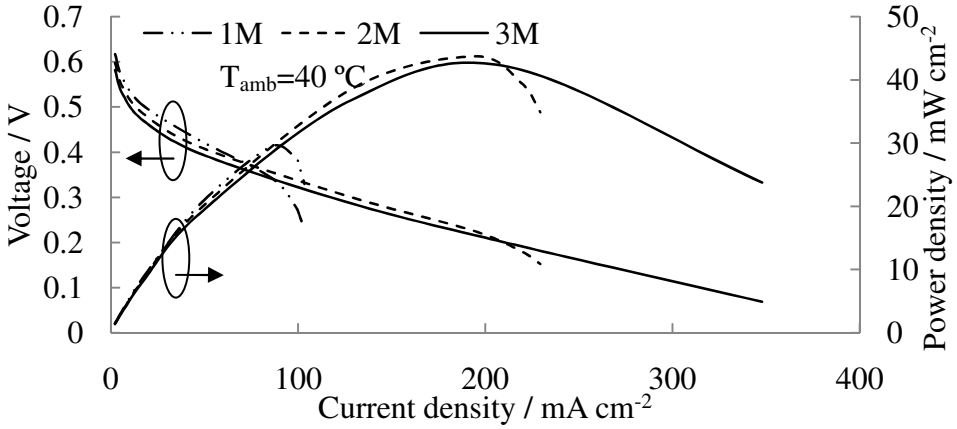

(b)

Figure 2.5: Polarization Curves for the Tubular DMFC Operated Passively with 1, 2, and 3 M Methanol Solutions at Different Ambient Temperatures: (a) 20 ºC and (b) 40 ºC.

Figure 2.5 shows the polarization curves during operation of the tubular, passive DMFC with 1 M, 2 M, and 3 M methanol solutions at 20 ºC and 40 ºC ambient temperatures. The main point of interest in this figure is to show how the performance of the fuel cell is affected by the ambient temperature. In real applications, the fuel cell must be able to operate similarly for several different, fluctuating ambient temperatures which may include indoor and outdoor operation, or even an extreme condition such as in a person's pocket that has the potential to increase the ambient temperature up to the body temperature (37 ºC). In order to prevent the limitation of oxygen along the axial direction of the CTL, each of these cases considers a 10 mm thick CTL (maximum CTL thickness). As expected and shown in Fig. 2.5, the performance of the fuel cell improves with each increase in external temperature, since the electrochemical kinetics at both the anode and cathode layers and the mass diffusion of species are dependent upon the temperature of the cell. Equations (56) and (60) represent the current density (A m^{-3}) at the anode and cathode, respectively. For a higher cell temperature, the exponential components of Eqs. (56) and (60) ($\frac{\alpha_a F \eta_a}{RT}$ and $\frac{\alpha_c F \eta_c}{RT}$), that consider the cell irreversibilities at the anode and cathode, are reduced. An increase in cell temperature means a decrease in the necessary activation energy at each catalyst layer and more favorable reactions at each side of the fuel cell. Another component of Eqs. (56) and (60) that is affected by a change in the cell temperature are the anode and cathode exchange current densities, $A_{v,a} J_{o,M}^{ref}$ and $A_{v,c} J_{o,O_2}^{ref}$, respectively. As seen by the equations for the anode and cathode exchange current densities found in previous work from the authors [3], both the anode and cathode exchange current densities increase as the cell temperature increases, which directly increase the anode and cathode current densities represented by Eqs. (56) and

(60) as well. The mass transport of methanol, water, and oxygen are also improved with an increase in cell temperature as seen in the diffusivity equations found in previous work from the authors [3]. With each increase in the external, ambient temperature, the steady-state operational temperature of the fuel cell associated with temperature rises due to phenomena including the latent heat of phase change, electrochemical reactions, and Joule heat will also increase.

As shown in Fig. 2.5(a), the maximum power density for an ambient air temperature of 20 ºC is 16.5 mW cm^{-2} with 1 M, 27.4 mW cm^{-2} with 2 M, and 32.7 mW cm^{-2} with 3 M methanol solution. As shown in Fig. 2.5(b), the maximum power density for an ambient temperature of 40 ºC is 18.8 mW cm^{-2} with 1 M, 38.6 mW cm^{-2} with 2 M, and 36.8 mW cm^{-2} with 3 M methanol solution. It is interesting to note that the peak power density for the 20 ºC ambient temperature case is for the 3 M methanol solution operation, but that the peak power density for the 40 ºC ambient air temperature case is for the 2 M methanol solution operation. The reason that the peak power density for the 3 M methanol operation only increases 4.1 mW cm^{-2} from the 20 ºC to the 40 ºC ambient air temperature case is that oxygen concentration is limited along the CTL and that a higher ambient temperature and subsequent cell temperature is associated with an increase in methanol crossover.

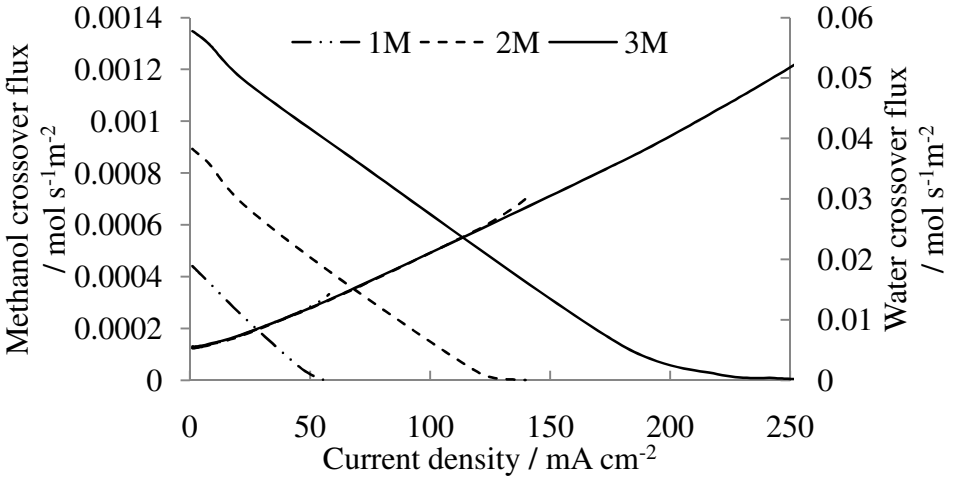

(a)

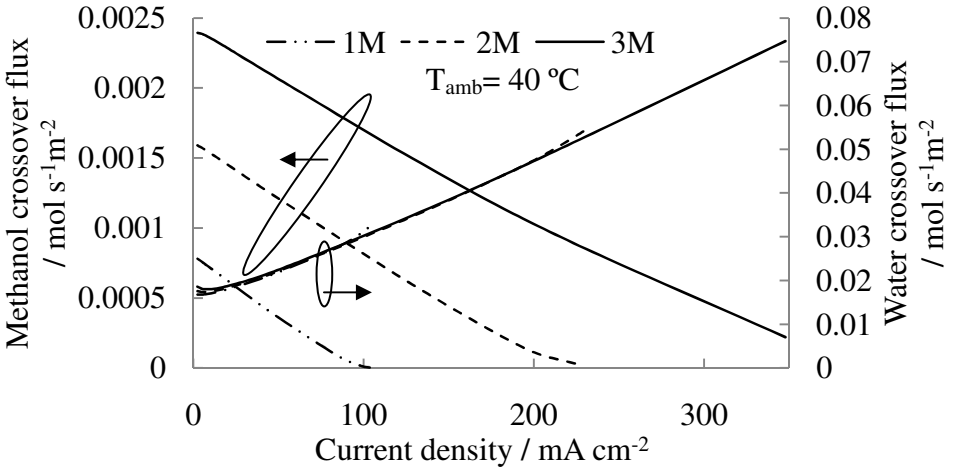

(b)

Figure 2.6: Methanol and Water Crossover Flux Due to Diffusion, Convection, and Electro-osmotic Drag for 1, 2, and 3 M Methanol Solutions at Different Ambient Temperatures: (a) 20 ºC and (b) 40 ºC.

Figure 2.6 shows the steady-state water and methanol crossover fluxes for a range of current densities and, also, considering operation at 20 ºC and 40 ºC ambient temperatures. Figure 2.6(a) shows the results for a 20 ºC ambient temperature, while Fig. 2.6(b) depicts the results for a 40 ºC ambient temperature. By comparing the results in both Figs. 2.6(a) and (b), it is apparent that the net methanol and water crossover increases as the ambient temperature increases. Considering Eqs. (12) and (13), which govern the sources of methanol and water crossover (diffusion, electro-osmotic drag, and convection), it is apparent that the main contributor to increased crossover as the temperature increases is diffusion. The diffusivity coefficient for methanol in Nafion® and dissolved water in Nafion®, as is documented in previous work from the authors [3], both increase by approximately 1.7 times as the ambient temperature increases from 20 ºC to 40 ºC. Moreover, during open circuit conditions (0 mA cm^{-2}), which is known to be the case in which diffusion is the dominant mode of crossover, Fig. 2.6(b) shows a significant increase in both methanol and water crossover compared to Fig. 2.6(a). Both figures then document a similar net crossover trend as the current density increases for both ambient cell temperatures, proving that the largest change in crossover is experienced during open circuit conditions at two different ambient temperatures.

These results are pertinent to the design and fabrication of a passively operated, tubular-shaped DMFC since the device must operate efficiently for a range of ambient temperatures. For example, if the fuel cell was installed into a portable application that was normally operated in room temperature environments then placed into a higher temperature environment (a pocket), it must be able to resist both water and methanol crossover (fuel loss) for both of these environments. Further work is needed to fully

understand methods of reducing the methanol and water crossover in changing ambient environmental temperatures.

2.5.3. Effect of CTL thickness

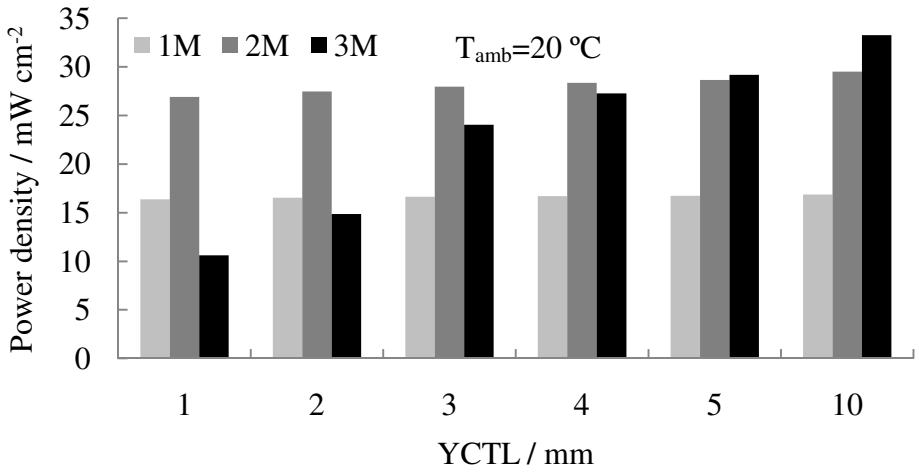

Figure 2.7: Maximum Attainable Power Density for each CTL Thickness: 1, 2, 3, 4, 5, and 10 mm with 1, 2, and 3 M Methanol Solutions at 20 ºC Ambient Temperature.

Based on the structure of a tubular-shaped, passive DMFC described in Fig. 2.2, the thickness of the CTL will affect the amount of oxygen from the air that can passively enter the CTL. To account for the "worst case scenario", the tubular-shaped, passive DMFC is operated at a peak power density (limiting current density) corresponding to each methanol solution while the thickness of the CTL is varied from 1 to 5 and 10 mm. Figure 2.7 shows a bar graph illustrating the effect that the CTL thickness has on the peak power density of the DMFC for 1, 2, and 3 M methanol solutions operated at a 20 ºC ambient air temperature. For the 1 M methanol solution case, the peak power density increases slightly from 16.4 to 16.9 mW cm^{-2} as the CTL thickness increases from 1 to 10 mm, respectively. On the other hand, for the 2 M methanol solution case, the peak power density increases from 26.9 to 29.5 mW cm^{-2}. For this case, there is also a net power density increase of 2.6 mW cm^{-2} from the smallest to the largest CTL thicknesses, and the most significant increase is from the 4 mm to the 5 mm thick CTL. Hence, it is assumed that the CTL should be at least 5 mm thick for 2 M methanol solution operation. Overall, for a 5 mm thick CTL, the performance of the DMFC operated with 1 and 2 M methanol solutions is not significantly affected by oxygen concentration limitations along the axial direction of the CTL. For the 3 M methanol solution case, the peak power density increases from 10.6 to 33.3 mW cm^{-2} as YCTL increases from 1 to 10 mm. This case represents the significant effect that oxygen depletion can have on the performance of the passively operated, tubular-shaped DMFC. During operation with 3 M or higher methanol solutions, the CTL must be at least 10 mm thick, if not larger, to account for the large consumption of oxygen at the cathode catalyst layer. However, to account for the

maximum ratio of tubular to planar VPD, the maximum CTL thickness is considered to be 10 mm, which results in a tubular VPD equal to the VPD of the planar DMFC.

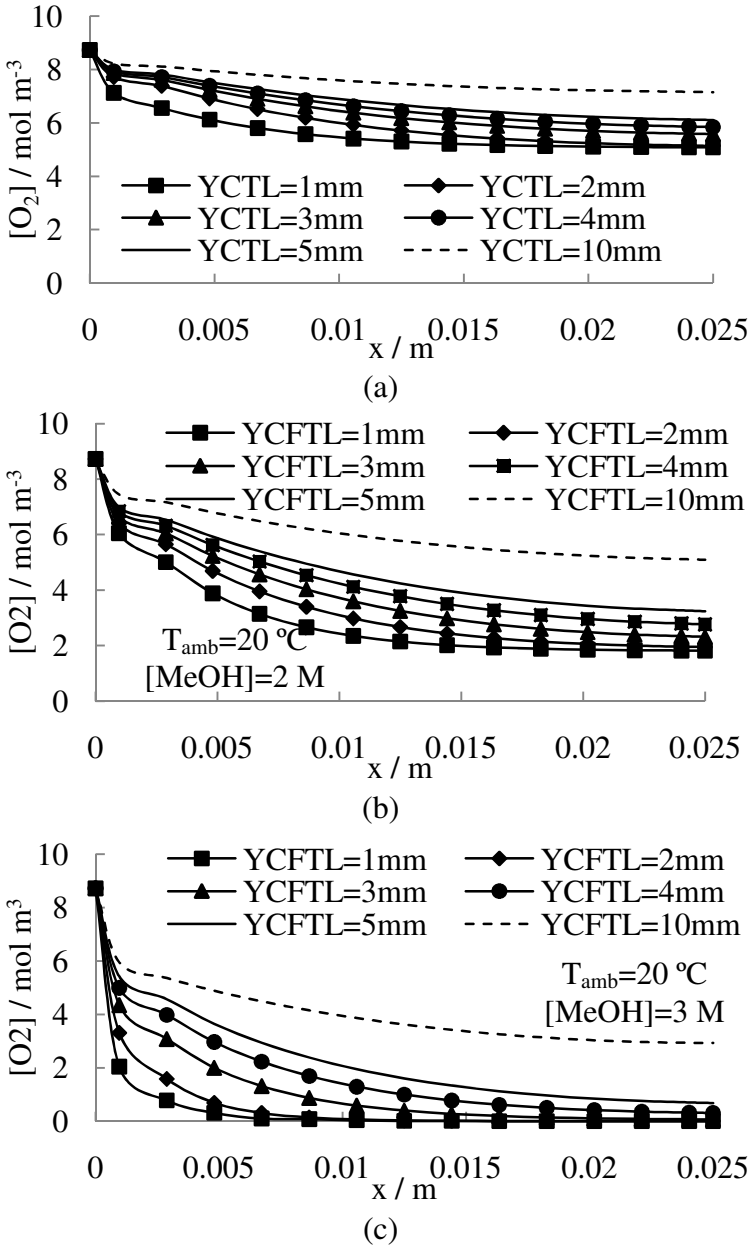

Figure 2.8: Steady-state Oxygen Concentration [O_2] Along the Axial Direction of the Tubular DMFC at the CTL/CDL Interface for (a) 1 M Methanol Solution at 55 mA cm^{-2}, (b) 2 M Methanol Solution at 126 mA cm^{-2}, and (c) 3 M Methanol Solution at 211 mA cm^{-2}.

Further in-depth analysis of the specific oxygen concentration along the CTL at the CDL interface is shown in Fig. 2.8 for different CTL thicknesses and methanol solutions as the cell is operated at the limiting current density for each methanol solution. As expected, the concentration of oxygen decreases from the entrance of the CTL, along the inside of the CTL to a minimum at the center of the CTL. Figure 2.8(a) shows the steady-state oxygen concentration during discharge at 55 mA cm^{-2} from the entrance of the CTL at x=0 to the center of the CTL at x=0.025m during operation with 1 M methanol solution and considering several CTL thicknesses (1 to 5 mm and 10 mm). Since symmetrical boundary conditions are considered along the Y direction, at the center of the fuel cell, the concentration of oxygen to the left of the boundary is identical to the concentration of oxygen to the right for all locations, x, along the channel. It is shown in Fig. 2.8(a) that for all thicknesses of the CTL during 1 M methanol solution operation that the oxygen concentration decreases slightly from the entrance to the center of the CTL, but that the oxygen concentration does not go below 5 mol m^{-3} for even the thinnest CTL (1 mm). In other words, a 1 mm thick CTL is large enough to provide sufficient oxygen to the fuel cell during all operation with 1 M methanol solution.

Figure 2.8(b) shows the oxygen concentration along the CTL at the CDL interface during operation with 2 M methanol solution at 126 mA cm^{-2}. The concentration of oxygen at the center of the CTL (furthest away from the entrance) is 1.95 mol m^{-3} for the 1 mm thick CTL, 2.32 mol m^{-3} for the 4 mm thick CTL, 2.77 mol m^{-3} for the 5 mm thick CTL, and 5.1 mol m^{-3} for the 10 mm thick CTL. Thus, as the thickness of the CTL increases the oxygen concentration at the CDL interface increases as well and the fuel cell can produce a higher power density for each voltage as shown in Fig. 2.7. During

operation with 2 M methanol solution, the CTL should be greater than or equal to 5 mm thick to prevent limiting the performance of the fuel cell.

Figure 2.8(c) shows the oxygen concentration along the CTL at the CDL interface during operation with 3 M methanol solution at 211 mA cm^{-2}. For this case, the concentration of oxygen along the CTL is clearly shown to be a limiting factor in the performance of the fuel cell. As seen in Fig. 2.6(a), the quantity of methanol crossover increases significantly as the concentration of methanol in the AFR increases, and, as a result, the crossover methanol consumes a large amount of oxygen at the cathode and contributes towards the depletion of oxygen along the CTL. For the 5 mm thick CTL, the concentration of oxygen at the center of the CTL is 0.7 mol m^{-3} and for the 10 mm thick CTL, the concentration of oxygen at the center of the CTL is 2.93 mol m^{-3}. Ideally, the thickness of the CTL should be greater than 10 mm during 3 M methanol solution operation in order to provide sufficient oxygen to the CDL. As a result of the CTL thickness, the tubular DMFC with a 10 mm thick CTL does not produce its true peak power density during 3 M methanol solution operation due to limiting oxygen transport along the CTL. In order to improve this problem, the thickness of the CTL would need to be increased, resulting in a reduced ratio of tubular to planar VPD. Thus, by operating the passive, tubular-shaped DMFC with methanol solution equal to or greater than 3 M and a 10 mm thick CTL that the performance of the fuel cell will be limited by the oxygen concentration along the CTL and subsequently the reaction at the cathode side of the fuel cell.

2.6. Conclusions

A two-dimensional, two-phase, non-isothermal model was developed to investigate the steady-state performance and optimum design characteristics of a tubular shaped, liquid-feed DMFC operating completely passively. Different operating parameters such as 20 ºC and 40 ºC ambient temperatures, inlet methanol concentrations from 1 to 3 M, and CTL thicknesses from 1 to 5 and 10 mm were considered to examine their affect on the overall peak performance of the tubular DMFC. The following conclusions are made:

- An increase in the ambient temperature increases the species transport and subsequent cell temperature, which increases the anode and cathode exchange current densities and decreases the anode and cathode irreversibilities, resulting in increased performance of the fuel cell.
- For the case of a passively operated, tubular-shaped DMFC with a 10 mm thick CTL, the peak power density produced by the fuel cell for a 20 ºC ambient temperature is during 3 M methanol operation. But when the ambient temperature is increased to 40 ºC that the 2 M methanol operation produces more power than the 3 M methanol operation due to oxygen limitations in the CTL and increased methanol crossover.
- An increase in the ambient temperature for a passively operated, tubular-shaped DMFC increases both the methanol and water crossover due to a higher diffusivity coefficient.

- It is important to consider the specific concentration of methanol solution and subsequent CTL thickness in order to optimize the tubular-shaped DMFC performance.
- For a 5 cm long, tubular-shaped DMFC, the thickness of the CTL must be greater than or equal to1 mm for 1 M methanol solution operation, greater than or equal to 5 mm for 2 M methanol solution operation, greater than or equal to 10 mm for 3 M, and the thickness of the CTL for operation with higher than 3 M methanol solution needs further consideration.

References

[1] Ward T, Xu C, Faghri A. Performance and design analysis of tubular-shaped passive direct methanol fuel cells. The International Journal of Hydrogen Energy 2011;36:9216-30.

[2] Xu C, Faghri A. Analysis of an active tubular liquid-feed direct methanol fuel cell. Journal of Power Sources 2010;196:6332-46.

[3] Xu C, Faghri A. Water Transport Characteristics in a Passive Liquid-Feed DMFC. International Journal of Heat and Mass Transfer 2010;53:1951-66.

[4] Bahrami H, Faghri A. Transport Phenomena in a Semi-Passive Direct Methanol Fuel Cell. International Journal of Heat and Mass Transfer 2010;53:2563-78.

[5] Bahrami H, Faghri A. Exergy Analysis of a Passive Direct Methanol Fuel Cell. Journal of Power Sources 2010;196:1191-204.

[6] Bahrami H, Faghri A. Transient Modeling of a Passive Direct Methanol Fuel Cell Using Pure Methanol. Journal of the Electrochemical Society 2010;157:B1762-76.

[7] Bahrami H, Faghri A. Water Management in a Passive DMFC Using Highly Concentrated Methanol Solution. Journal of Fuel Cell Science and Technology 2011;8:1-15.

[8] Faghri A, Zhang Y. Transport Phenomena in Multiphase Systems. Massachusetts: Academic Press; 2006.

Chapter 3. Performance characteristics of a novel tubular-shaped passive direct methanol fuel cell

3.1. Background

Considering the limited tubular-shaped DMFC experimental work documented in Table 3.1, a novel passive, tubular-shaped DMFC frame was designed and fabricated to hold the MEA layers together more effectively, prevent leakage, and reduce the internal resistance across the fuel cell. The frame also provides channels for passive air-breathing to the cathode and an Anode Fuel Reservoir (AFR) to hold methanol in the center of the frame. Two different conventional Membrane Electrode Assemblies (MEAs), one with a Nafion® 212 membrane and the other with a Nafion® 115 membrane, were installed in the tubular frame and the DMFC was tested with 1 M, 2 M, and 3 M methanol solutions completely passively. Polarization curves were generated for each methanol concentration and constant voltage tests were run to determine both the fuel and energy efficiencies. The results from the tubular-shaped DMFC tests were also compared with identical tests run on a passive, planar-shaped DMFC using identical MEA's. The proposed tubular-shaped, passively operated DMFC shows significant improvement over existing tubular-shaped DMFCs reported in the literature. This work was published in the Journal of Power Sources [1].

Table 3.1: Literature Review of Tubular DMFC Experimental Efforts

Investigator	Membrane	Anode/Cathode Locations[a]	Anode/Cathode Fuels	Operation	Performance	Comments
2004-Kunimatsu et. al [2]	Flemion® Tube	In/Out	1 M MeOH/Air	Semi-Passive	12 mW cm^{-2}	Good performance due to hot-pressing to keep layers of MEA together
2005-Qiao et. al [3]	Flemion® Tube	In/Out	2 M MeOH/Air	Passive	2 mW cm^{-2}	Impregnation-Reduction method to coat CCL, poor performance
2005-Qiao et. al [4]	Flemion® Tube	In/NA	3 M MeOH/NA	Half-Cell	NA	Impregnation-Reduction method to coat ACL, poor performance
2006-Qiao et. al [5]	Flemion® Tube	In/Out	2 M MeOH/Air	Passive	1.8 mW cm^{-2}	Temperature treatment associated with impregnation-reduction method is harmful to membrane
2006-Shao et. al [6]	Nafion® in Sol.	Out/In	MeOH/Air	Active	NA	All layers are dipped or sprayed onto the fuel cell
2006-Shao et. al [7]	Nafion® in Sol.	Out/In	0.25 M MeOH/Air	Semi-Passive	9 mW cm^{-2}	Good performance associated with conductive Titanium current collectors
2007-Yazici [8]	Nafion® Tube	In/Out	H_2/Air	Semi-Passive	NA	Good performance associated with shrink-tubing holding all MEA layers together, future DMFC testing with MeOH
2007-Yu et. al [9]	Perfluorinated Resin in Porous Silica Tube	In/Out	4 M MeOH/Air	Semi-Passive	10 mW cm^{-2}	Used a frame design to hold the MEA layers together and prevent leakage, poor membrane conductivity compared to Nafion®
Present Work [1]	Nafion® 212 and 115 membranes	In/Out	1, 2, 3 M MeOH/ Air	Passive	24.5 mW cm^{-2}	Advantages: frame, Nafion® membrane, passive, stainless steel current collectors

a: Inside the tubular DMFC (In) versus Outside of the tubular DMFC (Out).

3.2. Experimental description

3.2.1. Membrane electrode assembly

Figure 3.1 shows a schematic diagram of the proposed tubular-shaped, passive DMFC. Figure 3.2(a) includes a labeled diagram of the MEA. The MEA consists of a custom-designed CCM sandwiched between two GDLs. The CCM is made from both Nafion® 212 and 115 polymer electrolyte membranes coated with 5mg cm^{-2} PtRu as an anode catalyst layer and 5mg cm^{-2} Pt as a cathode catalyst layer from BCS Fuel Cells, Inc. in Texas. Considering the performance of previous tubular experimental efforts [2-10], a Nafion® membrane was chosen as the optimal material to use as a polymer electrolyte layer in the fuel cell over the Flemion tube [2-7] and the perfluorinated resin injected into the porous silica pipe [9] based on low methanol crossover and high proton conductivity.

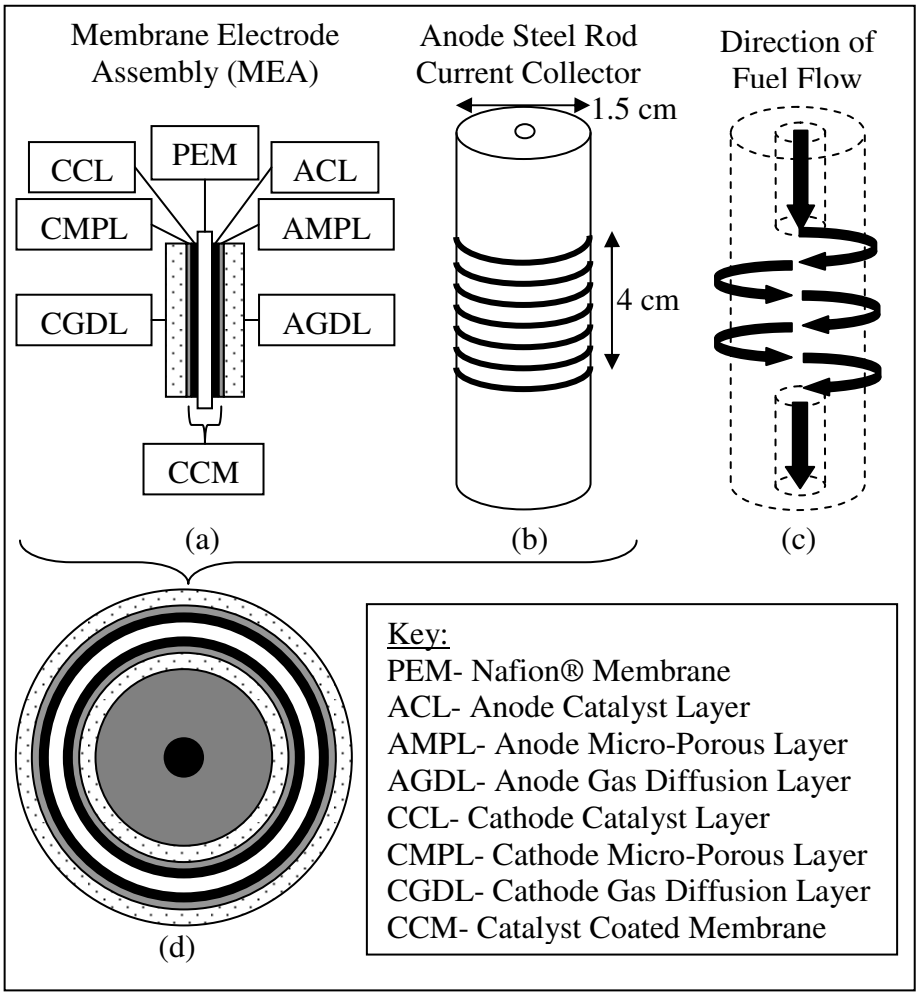

Figure 3.1: Diagram of the Tubular-shaped DMFC, Describing the (a) Layers of the MEA, (b) Anode Current Collector Rod, (c) Direction of Fuel Flow through the Anode Current Collector, and (d) MEA Wrapped Around the Inner Steel Rod Current Collector.

The CCM had to be custom designed so that it would fit into the tubular-shaped frame that had been designed and fabricated specifically for this experiment. The tubular CCM design included a 6x6 cm^2 Nafion® membrane with two different sized catalyst coated areas: the anode with a 4x5.3 cm^2 catalyst area and the cathode with a 4x5.6 cm^2 catalyst area. Since the CCM is wrapped around a steel rod during installation into the tubular-shaped DMFC frame, the actual area of the inner anode catalyst surface is smaller than the area of the external, cathode catalyst surface due to different radii as shown in Fig. 3.1(d). As a result, the tubular frame had to be designed, built, and tested to assure that the fuel cell would operate accordingly before the CCMs were designed and fabricated.

The area of the anode catalyst surface was estimated based on the circumferential area of the steel rod, with area added to account for expansion and contraction of the Nafion® membrane as it absorbs and expels water or methanol during testing. Covering both the anode and cathode catalyst layers, the GDLs are made from 50 % PTFE wet-proofed carbon cloth from Clean Fuel Cell Energy with a 4.6 mg cm^{-2} Micro-Porous Layer (MPL) loading coated in-house. The composition of the MPL is 25% Nafion® ionomer (Dupont 5% Nafion solution, 1100EW) and 75% carbon powder (Cabot brand Vulcan XC72R, GP-3860). MPL ink is produced by combining the Nafion® solution, carbon powder, and ethanol (as a solvent), then sonicating the solution for 30 minutes and applying the ink to the GDL via the "straight edge" technique. The "straight edge" technique includes using a dropper to add MPL ink directly onto the carbon cloth followed by using a flat, smooth edge (from a piece of metal, ruler, scraper, etc.) to evenly distribute the ink across the GDL. Following each application of ink to the GDL,

the carbon cloth is left to dry, weighed, and repeated as necessary to achieve the desired MPL loading. Finally, the GDL is placed in an oven at 350 ºC to sinter the carbon particles. The purpose of the MPL is to increase the mass transport resistance through the diffusion layer, to protect the catalyst layer, and also to add additional insulation to maintain an optimal cell temperature. The GDLs are sandwiched around the CCM with the MPLs in contact with each catalyst layer.

Prior to testing, the MEA is not hot-pressed. Instead, the MEA is pressed between two graphite current collectors in a 5x5 cm^2, planar, active fuel cell frame, which helps to press the three layers of the MEA together. The frame is heated to 80 ºC while 80 ºC distilled water is fed through the anode channels and 100 % humidified air at 80 ºC is fed through the cathode channels. The goal of this step, the hydration process, is to completely saturate the Nafion® membrane with water, which in turn reduces the internal resistance of the fuel cell by improving the proton conductivity of the membrane. This process is completed once the resistance across the MEA reduces to less than 15 mΩ (approximately 2 hours). Next, the MEA is activated by applying a constant voltage (0.6 V) load to the cell until a steady current density is produced from the fuel cell. First, the fuel cell frame is heated to 80 ºC while 100 % humidified hydrogen is fed through the anode channels at 0.8 L min^{-1} and 100 % humidified oxygen is fed through the cathode channels at 0.4 L min^{-1}.

After obtaining a steady current density from the fuel cell, a performance test is conducted to produce a polarization curve for the fuel cell during hydrogen and oxygen testing to compare against the performance from other MEAs. Next, the cell is cooled to 60 ºC and dilute methanol (~1 M) is fed through the anode channel at 1 ml min^{-1} while

room temperature air is fed through the cathode channel at 0.3 L min^{-1}. Again, a constant voltage (0.3 V) load is applied to the cell until a steady current density is produced and another performance test is run to produce a polarization curve for methanol and air. Finally, upon completion of the methanol and air testing, the active fuel cell frame is cooled to room temperature and the MEA is removed and installed into the tubular-shaped DMFC frame.

3.2.2. Tubular cell fixture

Considering the popularly used planar, passive DMFC structure, a tubular, passive DMFC frame was custom designed and fabricated to improve upon the existing performance of tubular DMFCs. The purpose of designing a passive, tubular-shaped DMFC frame is:

- To recreate testing conditions similar to those of the planar, passive DMFC, which has proven successful performance associated with a frame that houses the MEA.
- To provide sufficient, uniform, pressure across the MEA layers in order to reduce the overall internal resistance.
- To provide a strong central rod to wrap the MEA around, act as a current collector, and provide channels to transport methanol fuel to the anode side of the fuel cell.
- To provide an external current collector around the MEA with machined channels that allow sufficient passive air flow to the cathode side of the fuel cell.

- To provide insulation for the fuel cell to improve the kinetics at each catalyst layer.

The frame was initially fabricated from carbon, for conductive purposes, but later was rebuilt from stainless steel to account for structural strength. The electrical conductivity of stainless steel is slightly lower than that of carbon, but stainless steel has been used as a current collector in previous passive DMFC research because of its strength, resistance to corrosion, and good conductivity.

Figures 3.1(b) and 3.2(a) show the stainless steel rod that the MEA is wrapped around during installation. This rod acts as the anode current collector and also has a fuel channel machined in a helix pattern around the outside of the rod to allow methanol transport. Figure 3.1(c) shows the direction of methanol flow first axially through the center of the rod, then the methanol flows out of the center of the rod to the exterior of the rod and radially around the helix-shaped channel, and finally it returns to the center of the rod and exits axially out the bottom of the rod. During installation, the activated MEA is wrapped around the rod, with the anode gas diffusion layer in contact with the rod and covering the helix shaped fuel channel. The two adjoining edges of the MEA are separated by a piece of Polytetrafluoroethylene (PTFE) tape. PTFE Tape is also wrapped around either end of the MEA. The three locations of PTFE tape are described further in Fig. 3.2(d). The PTFE tape is used because:

- It creates a leak-proof seal along the adjoining edges of the MEA.
- It prevents the anode and cathode GDLs from touching and causing a short circuit.
- It is a good non-conductive, insulating, sticky material.

The total active area of the MEA is calculated based on the total surface area in contact between the anode GDL and the anode stainless steel rod. It is simply the surface area of the stainless steel rod in the region of the fuel channels minus the area of the piece of PTFE tape that connects the adjoining edges of the MEA. Using the dimensions shown in Fig. 3.1(b) and subtracting the area of the PTFE tape between the adjoining edges of the MEA, the total active area for the MEA is 13.77 cm^2.

The entire tubular fuel cell frame consists of three pieces: the inner stainless steel rod, which is used as the anode current collector, and an outer cathode current collector that is broken into two pieces. The outer part of the frame is also made from stainless steel and acts as the cathode current collector. In order to clamp down around the MEA, the outer section is designed as two pieces that fit together on opposite sides of the anode rod, around the MEA. Figure 3.2 shows a breakdown of the steps taken to construct the tubular fuel cell frame enclosing the MEA. The diameter of the inner anode steel rod is 1.5 cm and the diameter of the external steel portion of the frame that closes around the MEA and anode steel rod is 1.6 cm. Considering an average DMFC MEA to be 0.075 cm thick, this provides 0.05 cm between the inner anode steel rod and the exterior cathode current collector so that pressure is applied across the MEA layers as the outer cathode portion of the frame closes around the MEA.

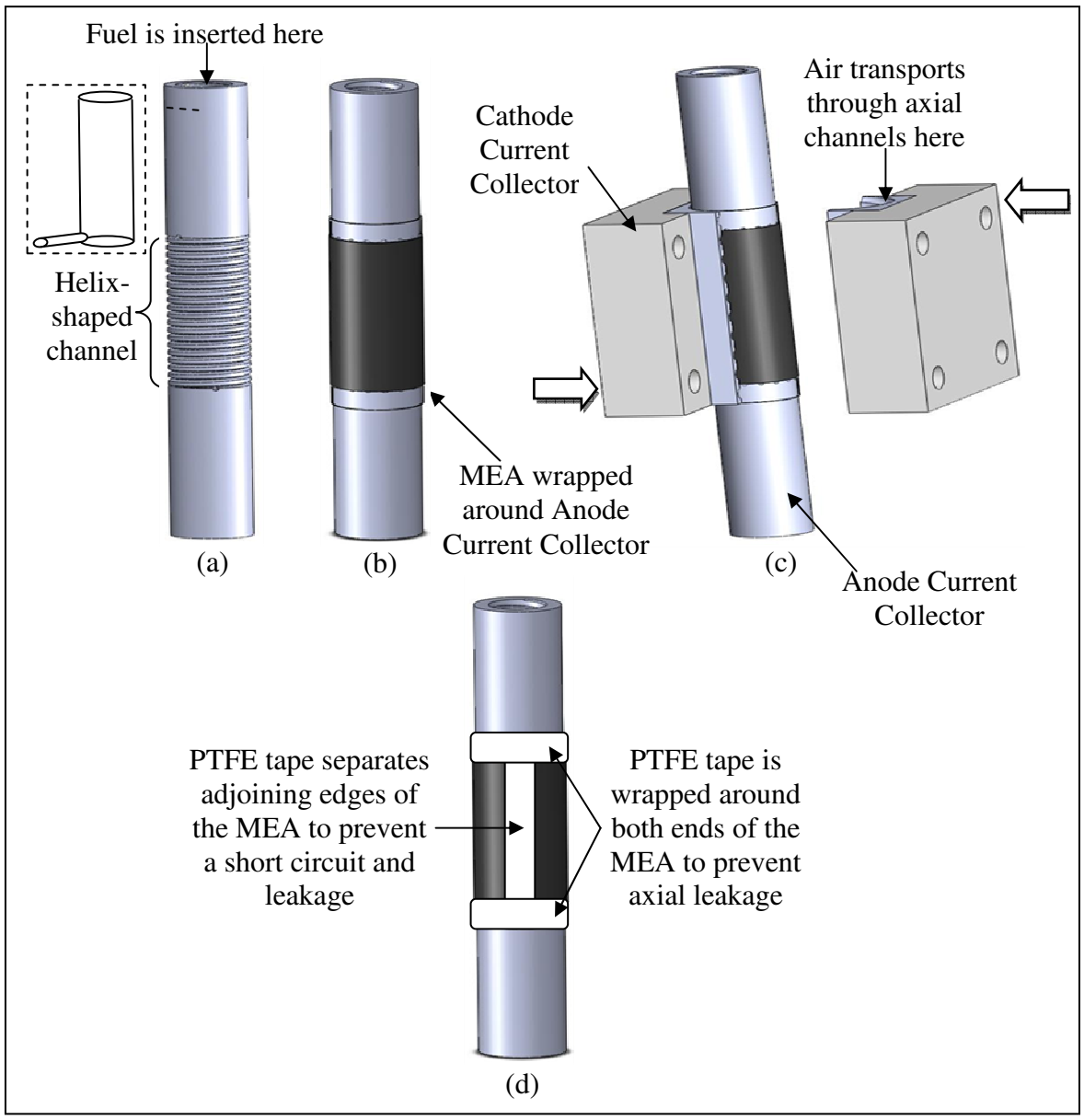

Figure 3.2: Schematic Showing the Steps to Build the Fuel Cell Frame Including the (a) Anode Current Collector rod with Helix-shaped Fuel Channel, (b) MEA Wrapped around the Helix-shaped Fuel Channel, (c) Cathode Current Collector Enclosing the MEA and Anode Current Collector, and (d) Three Locations of PTFE Tape.

Longitudinal air flow channels are machined into the cathode current collector pieces to allow sufficient passive air flow from the external ambient air to the cathode side of the fuel cell. The air flow channels are 5 mm deep, 2 mm wide, and travel the entire length of the frame to allow air entry or exit from either side of the frame. The outer portion of the fuel cell frame serves several purposes, including:

- Providing uniform pressure across the MEA to reduce the internal resistance.
- Acting as a current collector for the cathode side of the fuel cell.
- Providing channels for passive air transport to the cathode side of the fuel cell.
- Insulating the MEA to maintain a temperature higher than the ambient air, to improve the kinetics at each catalyst layer.
- Providing protection from external debris and dust that could hinder the performance of the fuel cell

3.2.3. Testing procedure

Once the MEA is installed into the tubular fuel cell frame, water is passed through the anode fuel channels to check for liquid-leaks. During the initial design/testing stages; leaks were a frequent problem associated with the tubular frame design, since there were three different locations that leaked fluid: the adjoining edges of the MEA when it is wrapped around the anode rod, and both ends of the MEA. Careful, meticulous installation of the MEA into the tubular frame and PTFE tape added between the adjoining edges of the MEA and wrapped around both ends of the MEA helped to prevent leaks. It is important to prevent leaks and install the MEA correctly during the

first installation to prevent degradation of the MEA caused by excessive contact and flexing of the MEA layers during repeated reinstallations.

A Multi Range Fuel Cell Test System from Scribner Associates (850e) was used to test the fuel cell by applying an adjustable, electronic load along the circuit connecting the anode and cathode. Anode and cathode electrical leads were connected to the central steel rod and exterior steel portion of the frame, respectively, to apply the load across the cell. The tubular DMFC was tested with 1 M, 2 M, and 3 M methanol solutions, since higher concentrations of methanol would result in methanol crossover and subsequent damage to the MEA due to de-lamination of the layers. Before the start of each test, methanol solution was injected into the AFR until the entire fuel channel was filled. During all of the tests, the fuel cell was operated with the anode steel rod pointing upward while the bottom of the rod was taped to hold the methanol solution in the rod during operation. The tape was removed upon the completion of each test to allow any excess fuel and water to drain from the AFR. Another reason that the steel rod was positioned vertically during testing was to allow generated carbon dioxide gas to escape through the AFR due to buoyancy forces. In between tests, air was forced through the anode fuel channel to remove all the liquid and carbon dioxide from the previous test. The fuel cell was stored overnight with distilled water in the AFR to maintain the water content in the membrane and to assure consistent performance the next day. Long-term, constant voltage tests and polarization curves were performed for each concentration of Methanol to validate the long-term performance of the fuel cell and to calculate the fuel and energy efficiencies of the tubular DMFC during completely passive operation. The polarization curves were measured after each fuel cell had achieved a steady open circuit

voltage following each new addition of methanol into the fuel cell reservoirs. A thermocouple was installed at the cathode side of the MEA, in the air channel contacting the GDL, to measure the temperature of the fuel cell during operation.

To perform a long-term constant voltage test, 2 ml of methanol solution was initially injected into the AFR. Next, a constant 0.35 V load was applied to the cell and the corresponding current density versus time was recorded until the cell had used up all of the methanol in the fuel reservoir and the current density reduced to zero. Considering the results from the long-term constant voltage tests for each methanol concentration, both the fuel and energy efficiencies of the DMFC with Nafion® 212 and Nafion® 115 membranes were calculated and compared with the fuel and energy efficiencies of a planar-shaped DMFC, also operated passively. The fuel efficiency is calculated by comparing the total current produced by the fuel cell to the actual total current that the fuel cell should produce based on a given volume of fuel [11]. This is represented by the following equation:

$$\eta_{\text{fuel}} = \frac{\int_0^{\text{t}} i(t)dt}{6C_{\text{m}}V_{\text{m}}F} * 100 \quad (1)$$

where $i(t)$ is the current produced by the fuel cell at a given time t integrated over the total time of the test, C_{m} is the concentration of methanol used in the cell, V_{m} is the volume of methanol injected into the anode fuel cell, and F is Faraday's Constant (96485 C mole^{-1}). The energy efficiency compares how much power the fuel cell produced to how much power is actually available in a given volume of fuel [11], and is represented by the following equation:

$$\eta_{\text{energy}} = \frac{V\int_0^{\text{t}} i(t)dt}{6C_{\text{m}}V_{\text{m}}FV_{\text{o}}} * 100 \quad (2)$$

where V is the operating voltage of the fuel cell (0.35 V) and V_o is the maximum cell voltage considering no irreversibilities (1.18 V).

A passive, planar DMFC with a 3x3 cm^2 active area was also tested with identical Nafion® 212 and 115 CCMs from BCS Fuel Cells, Inc with the same 5 mg cm^{-2} anode and cathode catalyst loadings. Similarly to the tubular DMFC, the planar DMFC was tested with 1 M, 2 M, and 3 M methanol solutions in identical conditions (room temperature, passive) to produce comparable results. To account for similar constant voltage experiment run times, unlike the tubular DMFC which was tested with 2 ml of Methanol, the planar DMFC was tested with 1.3 ml of Methanol. This volume was calculated by setting the ratio of fuel volume to active area for the tubular DMFC equal to the ratio of volume to active area for the planar DMFC. Table 3.2 provides a comparison summarizing of the performance results from the planar and tubular passive, DMFCs.

Table 3.2: Comparison of Planar and Tubular, Passive DMFCs

DMFC Type	Nafion® Membrane	[MeOH] / mole L^{-1}	Maximum Power Density / mW cm^{-2}	Limiting Current Density / mA cm^{-2}	Maximum Temperature Change / ºC[a]
Planar	212	1.0	8.3	25.7	1
		2.0	13.9	58.9	1
		3.0	20.0	124.1	3
	115	1.0	9.8	27.2	1
		2.0	20.2	59.9	2
		3.0	23.2	126.3	2
Tubular	212	1.0	10.6	42.5	1
		2.0	14.5	63.3	2
		3.0	19.0	115	3
	115	1.0	15.3	60.1	0
		2.0	19.4	90.4	1
		3.0	24.5	136	2

a: During Constant Voltage Discharge at 0.35 V.

3.3. Results and discussion

3.3.1. Performance

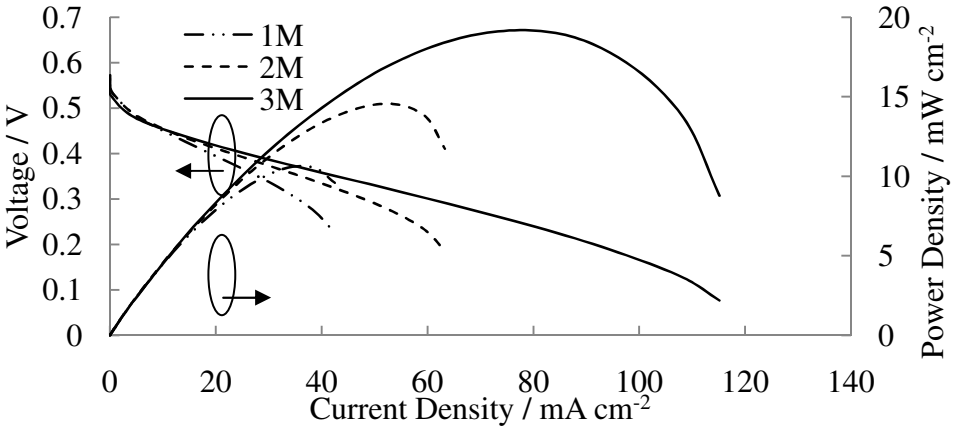

(a)

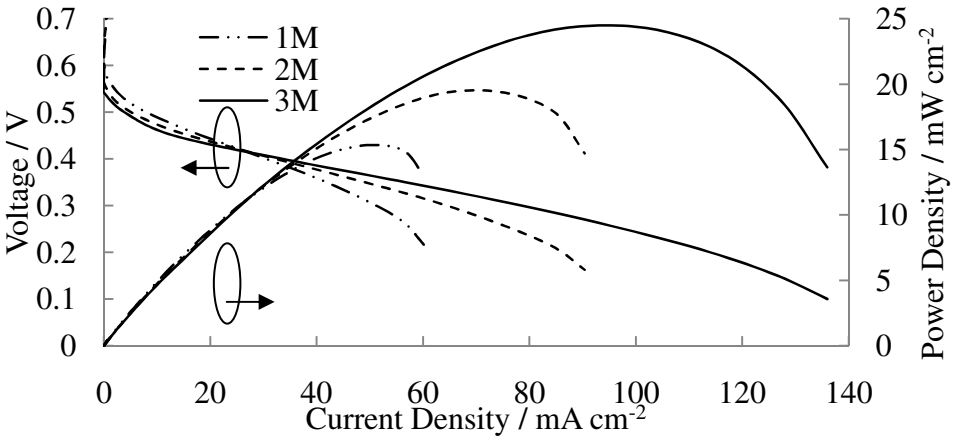

(b)

Figure 3.3: Passive, Tubular DMFC Polarization Curves for 1, 2, and 3 M Methanol Solutions Utilizing (a) a Nafion® 212 CCM and (b) a Nafion® 115 CCM.

Figure 3.3 represents the performance of the tubular DMFC during passive operation with 1 M, 2 M, and 3 M methanol solutions, respectively. Prior to each test, new methanol solution was injected into the AFR. Oxygen was provided by the air to the cathode side of the fuel cell. For both the Nafion® 212 and 115 MEAs, the performance of the tubular DMFC improved with each increase in methanol solution due to an increased methanol concentration at the ACL/Nafion® membrane interface. For example, the peak power density of the tubular DMFC increased from 10.6 to 19.0 mW cm^{-2} and from 15.3 to 24.5 mW cm^{-2} as the methanol concentration increased from 1 M to 3 M with the Nafion® 212 and 115 MEAs, respectively. With a larger concentration of fuel available at the ACL/Nafion® membrane interface, the anode irreversibilities were reduced, and as a result, the cell performance was improved. However, with a higher concentration of methanol, there is a higher quantity of methanol crossover from the anode to the cathode. Crossover methanol that reacts at the cathode side of the fuel cell produces large amounts of heat which, as a result, increases the temperature of the fuel cell. Methanol crossover ultimately results in decreased fuel efficiency, but an increase in cell temperature improves the kinetics at both the anode and cathode catalyst layers and, thus, the performance of the fuel cell.

The performance of the tubular DMFC is better with the Nafion® 115 MEA than with the Nafion® 212 MEA for all methanol concentrations. For the Nafion® 212 MEA, the maximum power densities were 10.6, 14.5, and 19.0 mW cm^{-2} with 1 M, 2 M, and 3 M methanol solutions, respectively. For the Nafion® 115 MEA, the maximum power densities were 15.3, 19.4, and 24.5 mW cm^{-2} with 1 M, 2 M, and 3 M methanol solutions, respectively. A Nafion® 212 membrane is thinner and has a lower resistance to proton

conductivity but will allow more methanol crossover. A Nafion® 115 membrane is thicker and has a higher resistance to proton conductivity, but will provide better resistance to methanol crossover than the Nafion® 212 membrane.

The main reason that the Nafion® 115 MEA performed better than the Nafion® 212 MEA was that the Nafion® 115 MEA allowed the fuel cell to achieve a much higher limiting current density for each corresponding voltage due to its resistance to methanol crossover. For the 3 M methanol solution case, the Nafion® 115 MEA's limiting current density was 136 mA cm^{-2} while that of the Nafion® 212 MEA was 115 mA cm^{-2}. For the 2 M methanol solution case, the Nafion® 115 MEA's limiting current density was 90.4 mA cm^{-2} while that of the Nafion® 212 MEA was 63.3 mA cm^{-2}. For the 1 M methanol solution case, the Nafion® 115 MEA's limiting current density was 60.1 mA cm^{-2} while that of the Nafion® 212 MEA was 42.5 mA cm^{-2}. Both the Nafion® 212 and 115 CCMs were custom made for these experiments; thus, another potential reason for the varied performance between these two membranes is fabrication error, which was initially seen by the non-uniform catalyst layer on the Nafion® 212 CCMs.

Identical tests were run with the planar DMFC to generate polarization curves for the same Nafion® 212 and 115 MEAs. Figure 5 represents the performance of the planar DMFC during passive operation with 1 M, 2 M, and 3 M methanol solutions, respectively. By comparing the peak performance, limiting current densities, and range of voltage for the tubular and planar geometries shown in Figs. 3.3 and 3.4, it is apparent that the tubular DMFC performed better than the planar DMFC. The tubular DMFC produced a higher power density than the planar DMFC for every methanol concentration using both Nafion® 212 and 115 MEAs. For example, the peak power density was 24.5

mW cm^{-2} for the tubular DMFC and 23.2 mW cm^{-2} for the planar DMFC operating with a Nafion 115 membrane and 3 M methanol solution. The tubular DMFC also produced a higher limiting current density than the planar DMFC for every methanol concentration and with both Nafion® 212 and 115 MEAs except for the Nafion® 212 MEA with 3 M methanol solution. The higher power density associated with the tubular DMFC compared to the planar DMFC can be attributed to the large constant pressure applied across the MEA, as well as, a higher temperature rise in the tubular cell associated with increased methanol crossover.

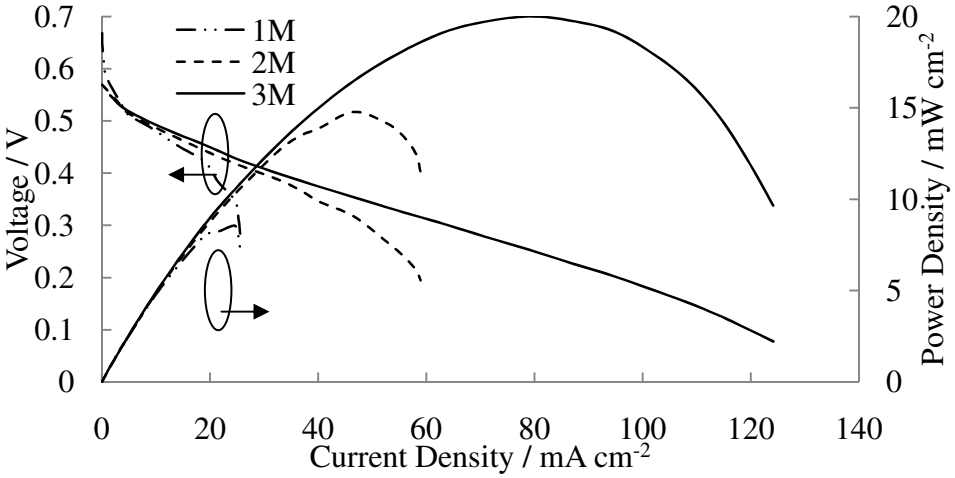

(a)

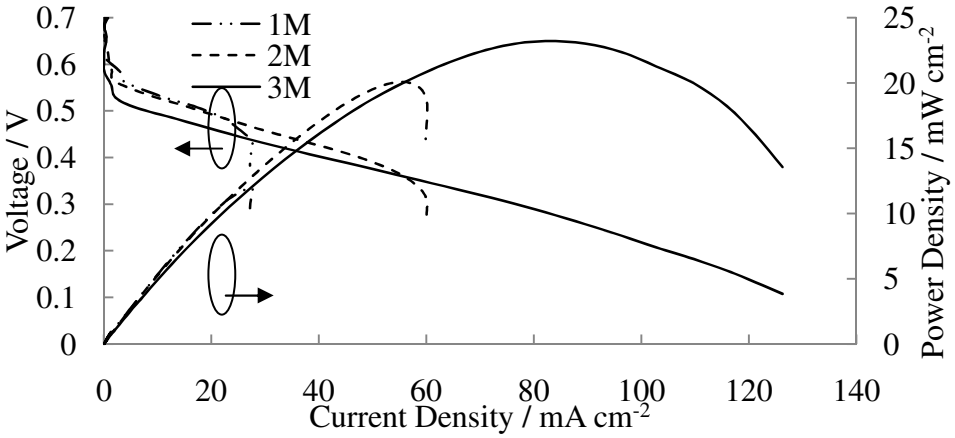

(b)

Figure 3.4: Passive, Planar DMFC Polarization Curves for 1, 2, and 3 M Methanol Solutions Utilizing (a) a Nafion® 212 CCM and (b) a Nafion® 115 CCM.

These results are very promising, since they show a significant improvement in performance for the passive, tubular DMFC. Based on the literature review, shown in Table 3.1, the previous best passive, tubular DMFC performance was 2 mW cm^{-2} with 2 M methanol solution [4] and the best semi-passive, tubular DMFC performance was 12 mW cm^{-2} with 1 M methanol solution [3]. In this work, a passive, tubular DMFC was designed and fabricated that produced 19.4 mW cm^{-2} with 2 M methanol solution and 15.3 mW cm^{-2} with 1 M methanol solution, which shows an 870 % improvement in power from the previous passive, tubular DMFC and a 27.5% improvement in power from the semi-passive, tubular DMFC. If the existing tubular DMFC is tested in a semi-passive mode, it should produce a much higher peak power density and limiting current density.

3.3.2. Constant voltage discharge

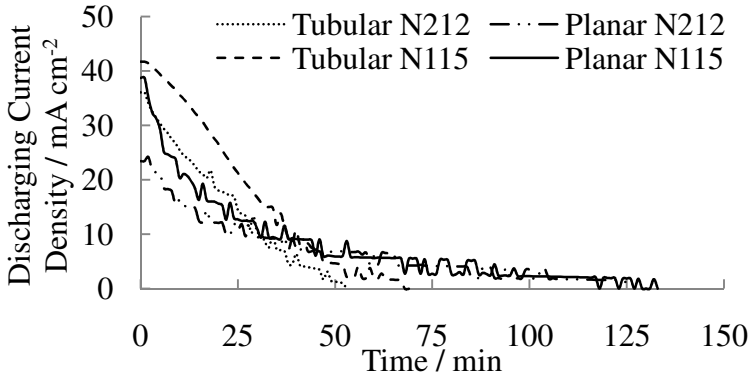

(a)

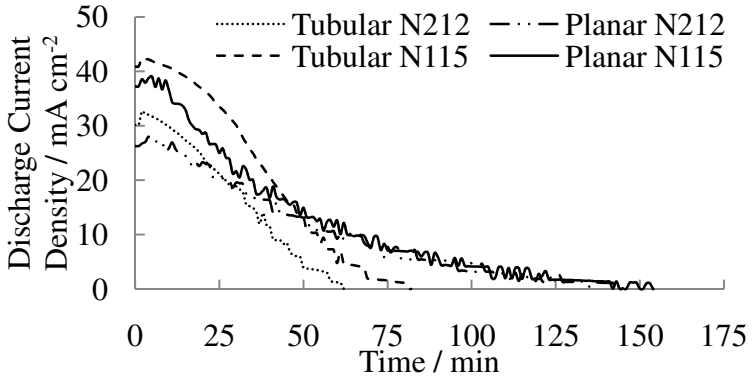

(b)

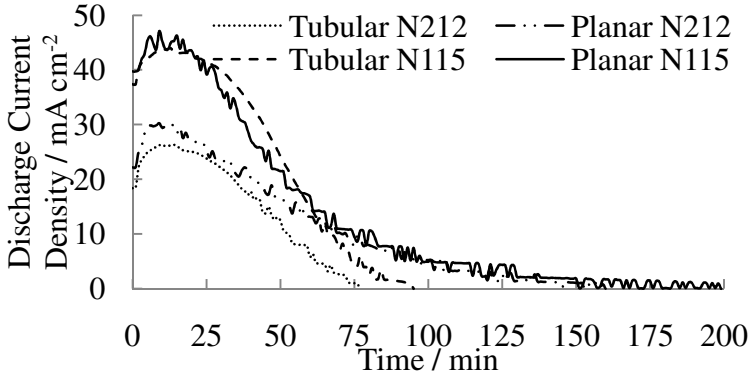

(c)

Figure 3.5: Variation of Tubular and Planar Constant Voltage (0.35 V) Discharge Current Density vs. Time with Nafion® 212 and 115 MEAs Utilizing (a) 1 M (b) 2 M and (c) 3 M Methanol Solutions.

Figure 3.5 presents the results from the constant voltage (0.35 V) tests with the tubular and planar DMFCs, respectively. Initially, 2 ml of methanol solution was injected into the AFR and the corresponding current density versus time was recorded and displayed in the figures. For each concentration of methanol, the planar DMFC operated for a longer period of time than the tubular DMFC. The results in Fig. 3.5 for the tubular DMFC all show a linear relationship between the discharging current density and time while the curves representing the planar DMFC follow more of an exponential decay.

Unlike the planar geometry, which has methanol resting on top of the MEA, the liquid methanol in the tubular DMFC is positioned in a vertical fuel channel then a helix-shaped channel, then another vertical channel at the bottom of the anode current collector. The tubular DMFC was tested with the anode rod positioned vertically to allow generated carbon dioxide gas to escape through the top of the rod. The vertical alignment of the tubular DMFC actually caused an increased methanol crossover with time due to a higher static fluid pressure in the tubular DMFC than in the planar DMFC. The height of the liquid methanol fuel in the planar AFR was less than 5 mm while the height of the fuel in the tubular AFR was 8 cm (height of the helix shaped channel plus the height of the central channel in the anode rod above the helix-shaped channel). Thus, the static fluid pressure at the bottom of the tubular DMFC is larger than the static fluid pressure in the planar DMFC.

With an increased static fluid pressure, the rate of methanol crossover in the tubular DMFC increased due to large pressure gradients across the Nafion® membrane. This explains why the discharging current density decreased to zero faster in the tubular DMFC than in the planar DMFC, because there was more fuel lost in the tubular DMFC.

It is worthwhile to note that the tubular DMFC produced an initial discharging current density similar to that of the planar DMFC, for all methanol concentrations, which reinforces the assertion that the tubular and planar DMFCs perform similarly. The main difference between the tubular and planar results, shown in Fig. 6, was that the tubular DMFC experienced significantly higher methanol crossover than the planar DMFC, which can be attributed to a higher static fluid pressure in the AFR.

The constant voltage discharge experiments with the Nafion® 115 MEA operated for a longer period of time than those with the Nafion® 212 MEA due to decreased methanol crossover associated with the thicker membrane. As the methanol is lost due to crossover, there is less fuel available, so the DMFC operates for a shorter period of time. The discharging current density for both the tubular and planar DMFCs was higher for the tests with the Nafion® 115 MEA than the tests with the Nafion® 212 MEA, once again due to decreased methanol crossover which produces higher performance from the fuel cell.

The tubular DMFC initially had a higher discharging current density than the planar DMFC for both Nafion® 212 and 115 MEA cases with 1 M and 2 M methanol solution, but during the 3 M methanol testing the planar geometry produced a higher initial discharging current density. One explanation for this is the geometry of the fuel cell. During construction of the tubular DMFC, an MEA is activated in a planar frame then wrapped around the central tubular rod which could induce stress fractures (cracks) in the MPL material initially applied and dried onto the GDL, and reduce the mass transport resistance of the MPL. Another explanation for the decreased discharging current density associated with the tubular DMFC and 3 M methanol solution is the

increase in methanol crossover with an increase in methanol concentration. It is worthwhile to note that the methanol crossover also increased in the planar DMFC as the concentration of methanol increased, but at a smaller rate than in the tubular DMFC. There are several other factors that could affect the methanol crossover in the tubular-shaped fuel cell compared to the planar-shaped fuel cell, including the possible differences in water crossover and liquid saturation at the catalyst layers for two geometries [12-14]. It should be noted that the higher static fluid pressure is only one potential explanation for the higher methanol crossover in the tubular-shaped fuel cell. Further research is required to fully understand the phenomenon affecting methanol crossover due to a change in geometry.

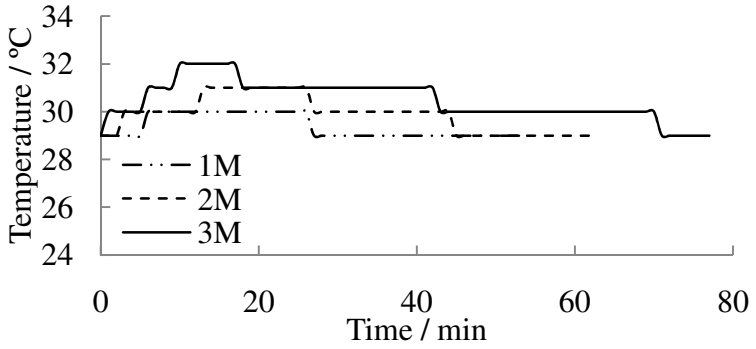

(a)

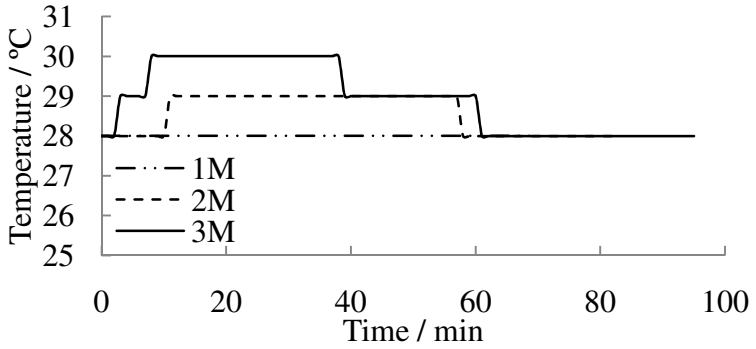

(b)

Figure 3.6: Tubular Temperature Profile during Constant Voltage Discharge Experiment with (a) a Nafion® 212 CCM and (b) a Nafion® 115 CCM.

Figure 3.6 presents the temperature of the tubular DMFC during the constant voltage discharge experiments starting from ambient temperature for each case. Due to an increased methanol crossover during testing with the Nafion® 212 MEA, the temperature increases for all methanol concentrations are higher during the constant voltage tests with the Nafion® 212 MEA than with the Nafion® 115 MEA. As methanol crosses over the membrane, it reacts at the cathode catalyst layer causing an increase in the cell temperature and also reducing the overall cell current density as reflected in Fig. 3.5, with the Nafion® 212 MEA discharges producing lower current density than the Nafion® 115 MEA discharges. It is also worthwhile to note that during the tubular DMFC constant discharge experiments that the change in cell temperature increased as the concentration of methanol increased. Operation with 3 M methanol solution produced a temperature change of 3 ºC and 2 ºC with Nafion® 212 and 115 MEAs, respectively, while operation with 1 M only produced a change of 1 ºC and 0 ºC with the Nafion® 212 and 115 MEAs, respectively.

3.3.3. Efficiency

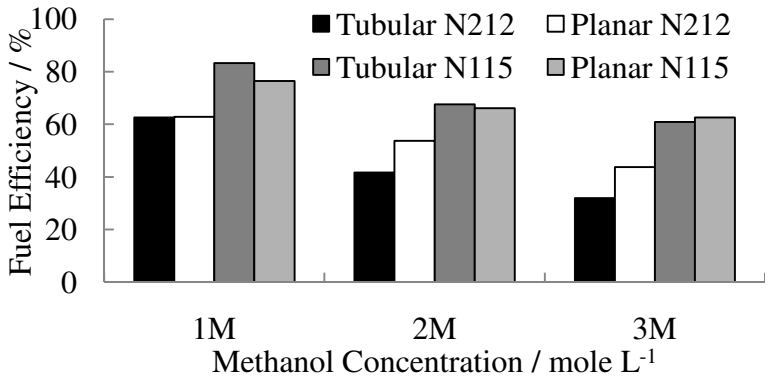

(a)

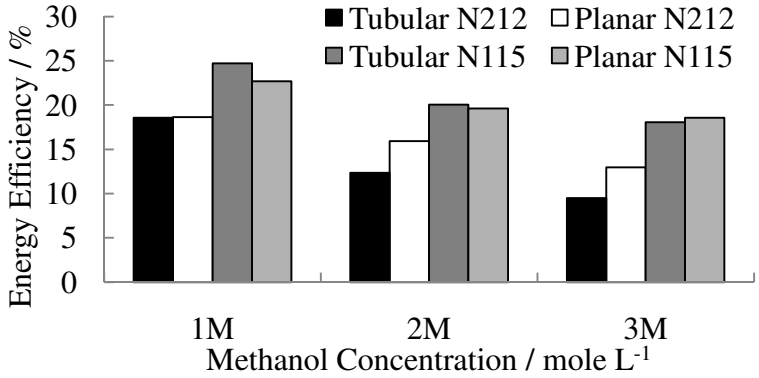

(b)

Figure 3.7: Comparing the (a) Fuel Efficiency and (b) Energy Efficiency of the Nafion® 212 and 115 Membranes in the Tubular and Planar DMFCs Operated Passively with 1, 2, and 3 M Methanol Solutions.

Following each constant voltage test, both the fuel and energy efficiencies of the tubular and planar DMFCs were calculated using Eqs. (1) and (2). Figure 3.7 presents the resulting fuel and energy efficiencies of the tubular and planar DMFCs with the Nafion® 212 and 115 MEAs, respectively. For both the tubular and planar DMFCs, the fuel and energy efficiencies are the greatest during operation with 1 M methanol solution and the least during operation with 3 M methanol solution due to methanol crossover that results in lost fuel and subsequently less available energy. For example, the fuel efficiency for the tubular DMFC with the Nafion® 212 MEA decreased from 62.6 % to 41.6 % to 32.0 % as the methanol concentration increased from 1 M, to 2 M, to 3 M. During operation with 1 M methanol solution, the least fuel crosses over both the Nafion® 212 and 115 membranes and is instead utilized at the anode to produce power, but as the methanol concentration increases, the quantity of methanol crossover also increases and the efficiency decreases.

For both the tubular and planar DMFCs, the fuel and energy efficiencies increase substantially for the Nafion® 115 MEA compared to the Nafion® 212 MEA. In the case of the tubular DMFC, the fuel efficiency for the Nafion® 212 MEA was 62.6 %, 41.6 %, and 32.0 % with 1 M, 2 M, and 3 M methanol solutions, respectively. However during operation with the Nafion® 115 MEA, the fuel efficiency for the tubular DMFC increased to 83.3 %, 67.6 %, and 60.8 % with 1 M, 2 M, and 3 M methanol solutions, respectively. Similarly to the fuel efficiency, the energy efficiency for the tubular DMFC decreased from 18.6 %, to 12.3 %, to 9.5 % with the Nafion® 212 MEA and from 24.7 %, to 20.0 %, to 18.0 % with the Nafion® 115 MEA during 1 M, 2 M, and 3 M operation, respectively.

Even though the fuel and energy efficiencies for both the tubular and planar DMFCs decrease as the methanol concentration increases, it is worthwhile to note that the difference between the fuel and energy efficiencies of the planar and tubular DMFCs increase significantly during 2 M and 3 M methanol solution operation and with the Nafion® 212 MEA. Initially, with the 1 M methanol solution, both the fuel and energy efficiencies of the tubular DMFC are similar to the fuel and energy efficiencies of the planar DMFC with the Nafion® 212 MEA, but as the methanol concentration increases to 2 M and then 3 M, the efficiencies of the planar DMFC become higher than the efficiencies of the tubular DMFC. For example, the fuel efficiency with the Nafion® 212 MEA decreased from 63.9 %, to 53.7 %, to 43.7 % for the planar DMFC, while the fuel efficiency for the tubular DMFC decreased from 62.6 %, to 41.6 %, to 32.0 %. The difference between the planar and tubular fuel efficiency increases as the methanol concentration increases, which means the tubular DMFC loses more fuel than the planar DMFC. The total run time of each constant voltage test also increased as the methanol concentration increased, due to more fuel available for the fuel cell to operate a longer period of time.

Considering the higher static fluid pressure in the tubular fuel cell than the planar fuel cell based on the orientation and structure of both cells, it is clear that as the run time increased that more methanol was lost due to crossover in the tubular fuel cell. This shows that the methanol crossover is also dependent upon time in the tubular fuel cell since both the fuel and energy efficiencies decreased as the methanol concentration, and associated run time, increased. Unlike the tubular DMFC, the planar DMFC was much more resistant to methanol crossover and maintained higher fuel and energy efficiencies

even as the methanol concentration and run time both increased. In other words, the methanol crossover is higher in the tubular DMFC than in the planar DMFC due to a higher static fluid pressure in the tubular AFR. Future efforts are needed to reduce the methanol crossover in the tubular fuel cell by increasing the mass transport resistance at the anode with the addition of another, lower porosity, gas diffusion layer.

3.4. Conclusions

A novel tubular-shaped, passive DMFC that operates with methanol solution in a central AFR and oxygen provided by the air was investigated. A tubular frame was designed and fabricated based on the existing planar, passive DMFC frame to provide fuel channels, current collectors, compression across the MEA, and to hold the MEA in a tubular shape. Nafion® 212 and 115 CCMs were used to produce MEAs with the addition of GDLs to either side of the CCM's. Also, a planar, passive DMFC was built and tested with identical MEAs for comparison. The following conclusions were made:

1. The performance of the Nafion® 115 MEA was better than that of the Nafion® 212 MEA due to decreased methanol crossover and reduced de-lamination of the MEA (attributed to methanol crossover).
2. The tubular DMFC produced 19.4 mW cm^{-2} with the 2 M methanol solution, which represents an 870% improvement in power from the previous best, passive, tubular DMFC.
3. The peak power density of the tubular DMFC was higher than that of the planar DMFC for both the Nafion® 212 and 115 MEAs operated with 1 M, 2 M, and 3 M methanol solutions.

4. The tubular DMFC produced equal fuel and energy efficiencies to those of the planar DMFC during 1 M methanol operation and with the Nafion® 212 MEA, but the fuel and energy efficiencies of the tubular DMFC were higher than those of the planar DMFC during the 1 M methanol operation and with the Nafion® 115 MEA.
5. The planar DMFC produced higher fuel and energy efficiencies than those of the tubular DMFC for both Nafion® 212 and 115 MEAs with 2 M and 3 M methanol solutions due to increased methanol crossover in the tubular fuel cell.
6. The tubular DMFC experienced higher methanol crossover than the planar DMFC potentially due to an increased static fluid pressure in the AFR caused by cell orientation and geometry.

References

[1] Ward T, Li X, Faghri A. Performance Characteristics of a Novel Tubular-Shaped Direct Methanol Fuel Cell. Journal of Power Sources 2011;196:6264-73.

[2] Kunimatsu M, Okada T. Performance of Microtubular DMFCs. Electrochemical and Solid-State Letters 2004; 7:A389-90.

[3] Qiao H, Kunimatsu M, Okada T. Pt Catalyst Configuration by a New Plating Process for a Micro Tubular DMFC Cathode. Journal of Power Sources 2005;139:30-4.

[4] Qiao H, Kunimatsu M, Fujiwara N, Okada T. Novel Heat-Treatment Process for Performance Enhancement of a Microtubular DMFC Anode Prepared by Impregnation-Reduction Method. Electrochemical and Solid-State Letters 2005;8:A175-8.

[5] Qiao H, Kasajima T, Kunimatsu M, Fujiwara N, Okada T. Evaluation of a Passive Microtubular Direct Methanol Fuel Cell with PtRu Anode Catalyst Layers Made by Wet Chemical Processes. Journal of the Electrochemical Society 2006;153:A42-7.

[6] Shao Z.G, Lin W.F, Zhu F, Christensen P.A, Zhang H, Yi B. A Tubular Direct Methanol Fuel Cell with Ti Mesh Anode. Journal of Power Sources 2006;160:1003-8.

[7] Shao Z.G, Lin W.F, Zhu F, Christensen P, Zhang H. Tubular Cathode Prepared by a Dip-Coating Method for Low Temperature DMFC. Fuel Cells 2006;6:326-30.

[8] Yazici M.S. Passive Air Management for Cylindrical Cartridge Fuel Cells. Journal of Power Sources 2007;166:137-42.

[9] Yu R.J, Cao G.Y, Liu X.Q, Li Z.F, Xing W, Zhu X.J. Fabrication of Support Tubular Proton Exchange Membrane for Fuel Cell. Journal of Fuel Cell Science and Technology 2007;4:520-4.

[10] Lee M, Chen L, Hung M, Lo M, Sue S, Lo C, Wang Y. A Novel Design of a Cylindrical Portable Direct Methanol Fuel Cell. Journal of Fuel Cell Science and Technology 2008;5:1-8.

[11] Liu J.G, Zhao T.S, Chen R, Wong C.W. The Effect of Methanol Concentration on the Performance of a Passive DMFC. Electrochemical Communications 2005;7:288-94.

[12] Bahrami H, Faghri A. Water Management in a Passive DMFC Using Highly Concentrated Methanol Solution. Journal of Fuel Cell Science and Technology 2011;8:1-15.

[13] Bahrami H, Faghri A. Transient Analysis of a Passive Direct Methanol Fuel Cell Using Pure Methanol. Journal of the Electrochemical Society 2010;157:B1762-76.

[14] Bahrami H, Faghri A. Transport phenomena in a semi-passive direct methanol fuel cell. International Journal of Heat and Mass Transfer 2010;53:2563-78.

Chapter 4: Future Work

4.1. Experimental

Until now, only low concentration (1-3 M) methanol solution has been tested in the passive, tubular-shaped DMFC. Initially, the goal was to build a tubular-shaped fuel cell that performed as well as existing planar fuel cells. Once this work was well established and the frame had been optimized, additional layers will now be added to the anode and cathode to allow high concentration operation. Building upon existing high concentration passive DMFC work [1-6], low porosity PTFE layers with a vaporizer layer constructed from Nafion® 117 membrane will be added to the anode to substantially increase the mass transport resistance of methanol from the fuel reservoir to the anode catalyst layer. Additional PTFE infused, carbon cloth, gas diffusion layers will be added to the cathode side of the fuel cell to promote the back diffusion of water from the cathode to the anode for diluting the methanol fuel at the catalyst layer.

A new frame will be fabricated at the local machine shop that allows variable thicknesses between the central anode rod current collector and external cathode portion of the frames. Currently, it is difficult to add additional layers around the central anode rod since the material will not fit in the allotted radial thickness provided by the external frame. Several options have been discussed with the machinists and are in the works of fabrication.

References

[1] Li X, Faghri A, Xu C. Water management of the DMFC passively fed with a high-concentration methanol solution. The International Journal of Hydrogen Energy 2010;35:8690-8.

[2] Xu C, Faghri A, Li X. Development of a High Performance Passive Vapor-Feed DMFC Fed with Neat Methanol. Journal of the Electrochemical Society 2010;157:B1109-17.

[3] Xu C, Faghri A, Li X. Improving the water management and cell performance for the passive vapor-feed DMFC fed with neat methanol. The International Journal of Hydrogen Energy 2011;36:8468-77.

[4] Li X, Faghri A. Effect of the cathode open ratios on the water management of a passive vapor-feed direct methanol fuel cell fed with neat methanol. Journal of Power Sources 2011;196:6318-24.

[5] Bahrami H, Faghri A. Water Management in a Passive DMFC Using Highly Concentrated Methanol Solution. Journal of Fuel Cell Science and Technology 2011;8:1-15.

[6] Xu C, Faghri A, Li X. Effect of the Structure Design on the Performance of a Passive Vapor-Feed DMFC Fed with Concentrated Methanol. ASME 2010 8th International Conference on Fuel Cell Science, Engineering and Technology (FUELCELL2010) 2010, pp. 51-57.

Appendix

A. Numerical nomenclature

[MeOH]	Methanol concentration, *mol L^{-1}*
[O_2]	Oxygen concentration, mol L^{-1}
A	Active area, *m^2*
A_{lg}	Specific interfacial area between liquid and gas phases, *m^{-1}*
$A_{v,a}J_{o,M}^{ref}$	Anode reference exchange current density, *A m^{-3}*
$A_{v,c}J_{o,O_2}^{ref}$	Cathode reference exchange current density, *A m^{-3}*
ACL	Anode catalyst layer
ADL	Anode diffusion layer
AFR	Anode fuel reservoir
AMPL	Anode micro-porous layer
a_W	Water vapor activity
MEA	Membrane electrode assembly
MEM	Nafion® polymer electrolyte membrane
C	Concentration of species, mol m^{-3}
C_p	Specific heat capacity, *J kg $^{-1}$ K^{-1}*
CCL	Cathode catalyst layer
CDL	Cathode diffusion layer
CMPL	Cathode micro-porous layer
CTL	Cathode transport layer
D	Diffusivity, *m^2 s^{-1}*
EW	Equivalent weight of the nafion® ionomer, *kg mol^{-3}*
F	Faraday's constant, *C mol^{-1}*
Gr	Grashof number
h	Interphacial transfer rate for methanol, *m^2 s^{-1}*
h_m	Mass transport coefficient, *m s^{-1}*
H	Height of planar stack, *m*
I	Current density, *A m^{-2}*
I_{cell}	Cell current, *A*
I_p	Parasitic current density, *A m^{-2}*
J_a	Anode current density, *A m^{-3}*
J_c	Cathode current density, *A m^{-3}*
k	Thermal conductivity
k_c	Condensation rate, *mol atm^{-1} s^{-1} m^{-3}*
k_e	Evaporation rate, *atm^{-1} s^{-1}*
k_r	Relative permeability, *m s^{-1}*
K	Permeability
L	Axial length of fuel cell/stack, *m*
$\dot{m}$	Rate of mass generation, *kg m^{-3} s^{-1}*
M	Molecular weight, *kg mol^{-1}*, Molar concentration, *mol L^{-1}*
MeOH	Methanol
n	Number of cells in a stack
n_d	Electro-osmotic drag coefficient
N	Molar Flux, *mol s^{-1}*
Nu	Nusselt number
P	Pressure, *atm*, or Power, *W*

Pr	Prandtl number
r_1	Radius of entire tubular fuel cell, m
r_2	Radius of anode catalyst layer, m
R	Universal gas constant, $J\ mol^{-1}\ K^{-1}$
$\check{R}$	Rate of phase change, $mol\ s^{-1}$
$\dot{R}$	Species source term, $mol\ m^{-3}\ s^{-1}$
R_{contact}	Ohmic contact resistance, $\Omega\ m^2$
s	Liquid saturation
$\bar{S}°$	Absolute entropy, $J\ mol^{-1}\ K^{-1}$
S	Source term
Sc	Schmidt number
Sh	Sherwood number
T	Temperature, K
u	Velocity in the x-direction, $m\ s^{-1}$
VPD	Volumetric Power Density, $mW\ m^3$
V	Velocity in the y-direction, $m\ s^{-1}$
V_0	Thermodynamic voltage, V
V_{cell}	Cell voltage, V
W	Width of stack, m
x	Molar fraction or Computational domain coordinate, m
y	Computational domain coordinate, m
Y	Thickness, m
$YACL$	Thickness of anode catalyst layer, m
$YADL$	Thickness of anode diffusion layer, m
$YAFR$	Thickness of anode fuel reservoir, m
$YAMPL$	Thickness of anode micro-porous layer, m
$YCCL$	Thickness of cathode catalyst layer, m
$YCDL$	Thickness of cathode diffusion layer, m
$YCMPL$	Thickness of cathode micro-porous layer, m
$YCTL$	Thickness of cathode transport layer, m

Greek

α	Transport coefficient
α_a	Anode transfer coefficient
α_c	Cathode transfer coefficient
γ	Reaction order of ORR
Γ	Effective diffusivity term
ε	Porosity or Nafion® volume fraction
η	Overpotential, V
λ	Water content in the membrane
θ	Contact angle, ^{o}
μ	Viscosity, $kg\ m^{-1}\ s^{-1}$
π	Pi, 3.14
ρ	Density, $kg\ m^{-3}$
σ	Nafion® membrane proton conductivity, $\Omega^{-1}\ m^{-1}$, or Surface tension, $N\ m^{-1}$
Δh	Latent heat of evaporation, $J\ mol^{-1}$

Superscripts

eff	Effective value
ref	Reference

sat	Saturated value
tank	Methanol fuel reservoir value
∞	Ambient air value

Subscripts

a	Anode
a/c	Anode or Cathode regions
acl	Anode catalyst layer
adl	Anode diffusion layer
ampl	Anode micro-porous layer
c	Cathode
ccl	Cathode catalyst layer
cell	Cell value
cdl	Cathode diffusion layer
cmpl	Cathode micro-porous layer
cr	Crossover
ctl	Cathode transport layer
CO_2	Carbon dioxide
Density	Density value
dry	Dry membrane value
e^-	Electron
g	Gas phase
H^+	Proton
H_2O	Water
l	Liquid phase
M	Methanol
MOR	Methanol oxidation reaction
mem	Membrane layer
N	Nafion®
O_2	Oxygen gas
ORR	Oxygen reduction reaction
planar	Referring to planar geometry
rg	Relative value for liquid phase
rl	Relative value for gas phase
stack	Stack value
T	Temperature
tubular	Referring to tubular geometry
v	Water vapor
vl	Vapor phase to liquid phase
W	Water
we	Dissolved phase

Appendix B

B. Numerical source and effective diffusivity terms for the governing equations

*Organized by layer: liquid pressure, gas pressure, species, energy

Parameter	Expression
Source Terms	S
ADL/AMPL	$\dot{m}_{\mathrm{l,a}} = M_{\mathrm{W}}\breve{R}_{\mathrm{vl}} - M_{\mathrm{M}}\breve{R}_{\mathrm{g,M}}$
	$\dot{m}_{\mathrm{g,a}} = -M_{\mathrm{W}}\breve{R}_{\mathrm{vl}} + M_{\mathrm{M}}\breve{R}_{\mathrm{g,M}}$
	$-\nabla\cdot\left(u_{\mathrm{l,a}}C_{\mathrm{M,l,a}}\right) + \dot{R}_{\mathrm{M,l,a}} = -\nabla\cdot\left(u_{\mathrm{l,a}}C_{\mathrm{M,l,a}}\right) - A_{\mathrm{lg}}h_{\mathrm{lg}}s(1-s)\dfrac{(P^{\mathrm{sat}}_{\mathrm{M,g}} - P_{\mathrm{M,g}})}{RT}$
	$-\nabla\cdot\left(u_{\mathrm{g,a}}C_{\mathrm{M,g,a}}\right) + \dot{R}_{\mathrm{M,g,a}} = -\nabla\cdot\left(u_{\mathrm{g,a}}C_{\mathrm{M,g,a}}\right) - A_{\mathrm{lg}}h_{\mathrm{lg}}s(1-s)\dfrac{(P^{\mathrm{sat}}_{\mathrm{M,g}} - P_{\mathrm{M,g}})}{RT}$
	$-\nabla\cdot\left(u_{\mathrm{g,a}}C_{\mathrm{W,g,a}}\right) + \dot{R}_{\mathrm{W,g,a}} = -\nabla\cdot\left(u_{\mathrm{g,a}}C_{\mathrm{W,g,a}}\right) - h_{\mathrm{vl}}(y_{\mathrm{wv}}P_{\mathrm{g}} - P^{\mathrm{sat}}_{\mathrm{W,g}})$
	$-\nabla\cdot\left(\rho_{\mathrm{l}}c_{\mathrm{p,l}}\vec{u}_{\mathrm{l}}T + \rho_{\mathrm{g}}c_{\mathrm{p,g}}\vec{u}_{\mathrm{g}}T\right) + S_{\mathrm{T}} = -\nabla\cdot\left(\rho_{\mathrm{l}}c_{\mathrm{p,l}}\vec{u}_{\mathrm{l}}T + \rho_{\mathrm{g}}c_{\mathrm{p,g}}\vec{u}_{\mathrm{g}}T\right) + (\breve{R}_{\mathrm{vl}}\Delta h_{\mathrm{v}} - \breve{R}_{\mathrm{g,M}}\Delta h_{\mathrm{g,M}})$
ACL	$\dot{m}_{\mathrm{l,a}} = M_{\mathrm{W}}\left(\breve{R}_{\mathrm{vl}} - \dfrac{N_{\mathrm{W,cr}}}{(YACL)} - \dfrac{J_{\mathrm{a}}}{6F}\right) - M_{\mathrm{M}}\left(\breve{R}_{\mathrm{g,M}} + \dfrac{J_{\mathrm{a}}}{6F} + \dfrac{I_{\mathrm{p}}}{6F(YACL)}\right)$
	$\dot{m}_{\mathrm{g,a}} = -M_{\mathrm{W}}\breve{R}_{\mathrm{vl}} + M_{\mathrm{M}}\breve{R}_{\mathrm{g,M}} + M_{\mathrm{CO_2}}\dot{R}_{\mathrm{CO_2,g}}$
	$-\nabla\cdot\left(u_{\mathrm{l,a}}C_{\mathrm{M,l,a}}\right) + \dot{R}_{\mathrm{M,l,a}} = -\nabla\cdot\left(u_{\mathrm{l,a}}C_{\mathrm{M,l,a}}\right) - \left(\breve{R}_{\mathrm{g,M}} + \dfrac{J_{\mathrm{a}}}{6F}\right)$
	$-\nabla\cdot\left(u_{\mathrm{g,a}}C_{\mathrm{M,g,a}}\right) + \dot{R}_{\mathrm{M,g,a}} = -\nabla\cdot\left(u_{\mathrm{g,a}}C_{\mathrm{M,g,a}}\right) + \breve{R}_{\mathrm{g,M}}$
	$-\nabla\cdot\left(u_{\mathrm{g,a}}C_{\mathrm{W,g,a}}\right) + \dot{R}_{\mathrm{W,g,a}} = -\nabla\cdot\left(u_{\mathrm{g,a}}C_{\mathrm{W,g,a}}\right) - \breve{R}_{\mathrm{vl}}$
	$-\nabla\cdot\left(\rho_{\mathrm{l}}c_{\mathrm{p,l}}\vec{u}_{\mathrm{l}}T + \rho_{\mathrm{g}}c_{\mathrm{p,g}}\vec{u}_{\mathrm{g}}T\right) + S_{\mathrm{T}}$
	$= -\nabla\cdot\left(\rho_{\mathrm{l}}c_{\mathrm{p,l}}\vec{u}_{\mathrm{l,a}}T + \rho_{\mathrm{g}}c_{\mathrm{p,g}}\vec{u}_{\mathrm{g,a}}T\right) + (J_{\mathrm{a}}\left(\eta_{\mathrm{a}} - \dfrac{T\Delta\bar{S}_{\mathrm{MOR}}}{6F}\right) + \dfrac{I^2}{\sigma_{\mathrm{mem}}} + \breve{R}_{\mathrm{vl}}\Delta h_{\mathrm{v}} - \breve{R}_{\mathrm{g,M}}\Delta h_{\mathrm{g,M}})$
MEM	$-\nabla\cdot\left(n_{\mathrm{d,W}}\dfrac{I}{F}\right) = -\nabla\cdot\left(\dfrac{2.5}{22}(\lambda)\dfrac{I}{F}\right)$
	$-\nabla\cdot\left(\rho_{\mathrm{l}}c_{\mathrm{p,l}}\vec{u}_{\mathrm{l}}T + \rho_{\mathrm{g}}c_{\mathrm{p,g}}\vec{u}_{\mathrm{g}}T\right) + S_{\mathrm{T}} = -\nabla\cdot\left(\rho_{\mathrm{l}}c_{\mathrm{p,l}}\vec{u}_{\mathrm{l}}T + \rho_{\mathrm{g}}c_{\mathrm{p,g}}\vec{u}_{\mathrm{g}}T\right) + \dfrac{I^2}{\sigma_{\mathrm{mem}}}$
CCL	$\dot{m}_{\mathrm{l,c}} = M_{\mathrm{W}}\left[\breve{R}_{\mathrm{vl}} + \dfrac{N_{\mathrm{W,cr}}}{(YCCL)} + \dfrac{J_{\mathrm{c}} - \dfrac{I_{\mathrm{p}}}{(YCCL)}}{2F} + \dfrac{I_p}{3F(YCCL)}\right]$
	$\dot{m}_{\mathrm{g,c}} = -M_{\mathrm{O_2}}\left(\dfrac{J_{\mathrm{c}}}{4F}\right) + M_{\mathrm{CO_2}}\left(\dfrac{I_{\mathrm{p}}}{6F(YCCL)}\right) - M_{\mathrm{W}}(\breve{R}_{\mathrm{vl}})$
	$-\nabla\cdot\left(u_{\mathrm{g,c}}C_{\mathrm{O_2,g,c}}\right) + \dot{R}_{\mathrm{O_2,g,c}} = -\nabla\cdot\left(u_{\mathrm{g,c}}C_{\mathrm{O_2,g,c}}\right) - \dfrac{J_{\mathrm{c}}}{4F}$
	$-\nabla\cdot\left(u_{\mathrm{g,c}}C_{\mathrm{W,g,c}}\right) + \dot{R}_{\mathrm{W,g,c}} = -\nabla\cdot\left(u_{\mathrm{g,c}}C_{\mathrm{W,g,c}}\right) - \breve{R}_{\mathrm{vl}}$
	$-\nabla\cdot\left(\rho_{\mathrm{l}}c_{\mathrm{p,l}}\vec{u}_{\mathrm{l}}T + \rho_{\mathrm{g}}c_{\mathrm{p,g}}\vec{u}_{\mathrm{g}}T\right) + S_{\mathrm{T}}$
	$= -\nabla\cdot\left(\rho_{\mathrm{l}}c_{\mathrm{p,l}}\vec{u}_{\mathrm{l,c}}T + \rho_{\mathrm{g}}c_{\mathrm{p,g}}\vec{u}_{\mathrm{g,c}}T\right) + (J_{\mathrm{c}}\left(\eta_{\mathrm{c}} - \dfrac{T\Delta\bar{S}_{\mathrm{ORR}}}{4F}\right) - \dfrac{I_{\mathrm{p}}T\Delta\bar{S}_{\mathrm{MOR}}}{6F(YCCL)} + \dfrac{I^2}{\sigma_{\mathrm{mem}}} + \breve{R}_{\mathrm{vl}}\Delta h_{\mathrm{v}})$
CDL/CMPL	$\dot{m}_{\mathrm{l,c}} = M_{\mathrm{W}}\breve{R}_{\mathrm{vl}}$
	$\dot{m}_{g,c} = -M_W\breve{R}_{vl}$
	$-\nabla\cdot\left(u_{\mathrm{g,c}}C_{\mathrm{O_2,g,c}}\right) + \dot{R}_{\mathrm{O_2,g,c}} = -\nabla\cdot\left(u_{\mathrm{g,c}}C_{\mathrm{O_2,g,c}}\right)$
	$-\nabla\cdot\left(u_{\mathrm{g,c}}C_{\mathrm{W,g,c}}\right) + \dot{R}_{\mathrm{W,g,c}} = -\nabla\cdot\left(u_{\mathrm{g,c}}C_{\mathrm{W,g,c}}\right) - \breve{R}_{\mathrm{vl}}$
	$-\nabla\cdot\left(\rho_{\mathrm{l}}c_{\mathrm{p,l}}\vec{u}_{\mathrm{l,c}}T + \rho_{\mathrm{g}}c_{\mathrm{p,g}}\vec{u}_{\mathrm{g,c}}T\right) + S_{\mathrm{T}} = -\nabla\cdot\left(\rho_{\mathrm{l}}c_{\mathrm{p,l}}\vec{u}_{\mathrm{l,c}}T + \rho_{\mathrm{g}}c_{\mathrm{p,g}}\vec{u}_{\mathrm{g,c}}T\right) + \breve{R}_{\mathrm{vl}}\Delta h_{\mathrm{v}}$
Effective Diffusivity Terms:	Γ
ADL/AMPL	$\rho_{\mathrm{l}}\left(-K\dfrac{K_{\mathrm{rl}}}{\mu_{\mathrm{l}}}\right)$
	$\rho_g\left(-K\dfrac{K_{\mathrm{rg}}}{\mu_{\mathrm{g}}}\right)$
	$D^{\mathrm{eff}}_{\mathrm{M,l,a}} = D_{\mathrm{M,l}}\varepsilon^{1.5}s^{1.5}$
	$D^{\mathrm{eff}}_{\mathrm{M,g,a}} = D_{\mathrm{M,g}}\varepsilon^{1.5}(1-s)^{1.5}$
	$D^{\mathrm{eff}}_{\mathrm{W,g,a}} = D_{\mathrm{W,g}}\varepsilon^{1.5}(1-s)^{1.5}$
	$k^{\mathrm{eff}}_{\mathrm{T}} = \varepsilon s k_{\mathrm{l}} + \varepsilon(1-s)k_{\mathrm{g}} + k_{\mathrm{adl}}$

Appendix B

ACL	$\rho_{\mathrm{l}}\left(-K\frac{K_{\mathrm{rl}}}{\mu_{\mathrm{l}}}\right)$
	$\rho_{g}\left(-K\frac{K_{\mathrm{rg}}}{\mu_{\mathrm{g}}}\right)$
	$D_{\mathrm{M,l,a}}^{\mathrm{eff}}=\frac{\varepsilon+\varepsilon_{\mathrm{e}}}{\left(\frac{\varepsilon}{D_{\mathrm{M,l}}\varepsilon^{1.5}s^{1.5}}\right)+\left(\frac{\varepsilon_{\mathrm{e}}}{D_{\mathrm{M,N}}\varepsilon_{\mathrm{e}}^{1.5}}\right)}$
	$D_{\mathrm{M,g,a}}^{\mathrm{eff}}=D_{\mathrm{M,g}}\varepsilon^{1.5}(1-s)^{1.5}$
	$D_{\mathrm{W,g,a}}^{\mathrm{eff}}=D_{\mathrm{W,g}}\varepsilon^{1.5}(1-s)^{1.5}$
	$k_{\mathrm{T}}^{\mathrm{eff}}=\varepsilon s k_{\mathrm{l}}+\varepsilon(1-s)k_{\mathrm{g}}+k_{\mathrm{acl}}$
MEM	$D_{\mathrm{W,N}}\frac{\rho_{\mathrm{dry}}}{EW}$
	$k_{\mathrm{T}}^{\mathrm{eff}}=k_{\mathrm{mem}}$
CCL	$\rho_{\mathrm{l}}\left(-K\frac{K_{\mathrm{rl}}}{\mu_{\mathrm{l}}}\right)$
	$\rho_{g}\left(-K\frac{K_{\mathrm{rg}}}{\mu_{\mathrm{g}}}\right)$
	$D_{\mathrm{O_2,g,c}}^{\mathrm{eff}}=D_{\mathrm{O_2,g}}\varepsilon^{1.5}(1-s)^{1.5}$
	$D_{\mathrm{W,g,c}}^{\mathrm{eff}}=D_{\mathrm{W,g}}\varepsilon^{1.5}(1-s)^{1.5}$
	$k_{\mathrm{T}}^{\mathrm{eff}}=\varepsilon s k_{\mathrm{l}}+\varepsilon(1-s)k_{\mathrm{g}}+k_{\mathrm{ccl}}$
CDL/CMPL	$\rho_{\mathrm{l}}\left(-K\frac{K_{\mathrm{rl}}}{\mu_{\mathrm{l}}}\right)$
	$\rho_{g}\left(-K\frac{K_{\mathrm{rg}}}{\mu_{\mathrm{g}}}\right)$
	$D_{\mathrm{O_2,g,c}}^{\mathrm{eff}}=D_{\mathrm{O_2,g}}\varepsilon^{1.5}(1-s)^{1.5}$
	$D_{\mathrm{W,g,c}}^{\mathrm{eff}}=D_{\mathrm{W,g}}\varepsilon^{1.5}(1-s)^{1.5}$
	$k_{\mathrm{T}}^{\mathrm{eff}}=\varepsilon s k_{\mathrm{l}}+\varepsilon(1-s)k_{\mathrm{g}}+k_{\mathrm{cdl}}$
CTL	$\rho_{\mathrm{l}}\left(-K\frac{K_{\mathrm{rl}}}{\mu_{\mathrm{l}}}\right)$
	$\rho_{g}\left(-K\frac{K_{\mathrm{rg}}}{\mu_{\mathrm{g}}}\right)$
	$D_{\mathrm{O_2,g,c}}^{\mathrm{eff}}=D_{\mathrm{O_2,g}}\varepsilon^{1.5}(1-s)^{1.5}$
	$D_{\mathrm{W,g,c}}^{\mathrm{eff}}=D_{\mathrm{W,g}}\varepsilon^{1.5}(1-s)^{1.5}$
	$k_{\mathrm{T}}^{\mathrm{eff}}=\varepsilon s k_{\mathrm{l}}+\varepsilon(1-s)k_{\mathrm{g}}+k_{\mathrm{CTL}}$